Professur für Hydrologie

der Albert-Ludwigs-Universität Freiburg i. Br.

Daniel Robert Eilertz

The linkage between meteorological drought indicators and streamflow patterns across Europe

Referent: Dr. Kerstin Stahl

Korreferent: PD Dr. Jens Lange

Masterarbeit unter der Leitung von Dr. Kerstin Stahl

Ehrenwörtliche Erklärung:

Hiermit erkläre ich, dass die Arbeit selbständig und unter Verwendung der angegebenen Hilfsmittel angefertigt wurde.

Freiburg im Breisgau, 8.November 2013 Daniel Robert Eilertz

Contents

List of Figures iii

List of Tables v

Abstract vii

Zusammenfassung ix

1 Introduction 1

1.1 Background 1

1.1.1 Meteorological drought indicators 1

1.1.2 Controlling factors on streamflow generation 3

1.1.3 Linking meteorological drought indicators with hydrological variables 4

1.2 Motivation and Objectives 5

2 Data and study area 7

2.1 Drought indices 7

2.1.1 Initial dataset 7

2.1.2 Time series computation of the SPEI 7

2.2 Discharge data 7

2.2.1 Runoff time series of near-natural and mesoscale catchments 7

2.2.2 Catchment geodata 8

2.2.3 Quality assessment 8

3 Methods 11

3.1 Computation of the Standardized Streamflow Index 11

3.1.1 Implementation of different distributions functions 11

3.1.1.1 Generalized Extreme Value distribution 12

3.1.1.2 Pearson type III distribution 13

3.1.1.3 Log-logistic distribution 13

3.1.1.4 Weibull distribution 14
3.1.1.5 Lognormal distribution 14
3.1.1.6 Generalized Pareto distribution 15
3.1.2 Parameter estimation based on L-Moments 16
3.1.3 Conversion to standardized z-scores 17
3.1.4 Goodness-of-fit test: Best Monthly Fit approach 17
3.2 Assessing the linkage between the SPEI and the SSI 18
3.2.1 Correlation analysis 18
3.2.2 Cluster analysis of the continuous correlations 19
3.2.3 Calculation of hydrological regimes 20
3.2.4 Correlation and cluster analysis of the monthly SPEI and SSI series 22
4 Results 23
4.1 Overall relationship between the SSI and the SPEI 23
4.2 Maximum correlation per catchment 26
4.3 Clusters of linkages of continuous series 33
4.4 Hydrological regimes 37
4.5 Monthly correlation patterns between the SPEI and the SSI 43
5 Discussion 55
5.1 Continuous relations between the SPEI and the SSI 55
5.2 Seasonal relations between the SPEI and the SSI 58
6 Conclusion 65
References 67
Abbreviations 72
Symbols 73

List of Figures

Figure 4.1: Correlations between continuous series of the SSI and the SPEI at different time scales in relation to different streamflow conditions. 23

Figure 4.2: Box plots of correlations between continuous series of the SSI and the SPEI at different time scales for each country. 25

Figure 4.3: Maximum strength of the correlation between both indicators and the respective SPEI time scales (1-12 months) for the complete period of observation. 27

Figure 4.4: Maximum strength of the correlation between both indicators and the respective SPEI time scales (1-12 months) during non-drought conditions. 28

Figure 4.5: Maximum strength of the correlation between both indicators and the respective SPEI time scales (1-12 months) during periods of streamflow drought. 29

Figure 4.6: Maximum strength of the correlation between both indicators and the respective SPEI time scales (1-12 months) during periods of mild streamflow drought. 30

Figure 4.7: Maximum strength of the correlation between both indicators and the respective SPEI time scales (1-12 months) during periods of moderate streamflow drought. 31

Figure 4.8: Progressions of obtained *r*-values over varying time scales of the SPEI for each cluster (C_C) of the continuous correlation. The 5^{th}, 25^{th}, 50^{th} and 95^{th} percentiles are indicated by transparency. 34

Figure 4.9: Box plots for mean values of surface area, elevation, slope, rainfall and temperature for those catchments represented by each cluster (C_C) of the continuous correlation analysis. 35

Figure 4.10: Spatial distribution of the clusters (C_C) of the continuous correlation analysis. 36

Figure 4.11: Runoff regimes (C_r) of the clustered catchments. The 5th, 25th, 50th and 95th percentiles of monthly Pardé-coefficients are indicated by transparency. 38

Figure 4.12: Location of the catchments represented by each runoff regime (C_r)..... 39

Figure 4.13: Box plots of correlations between continuous series of the SSI and the SPEI at different time scales for each runoff regime (C_r)..... 41

Figure 4.14: Correlation patterns of the monthly SSI and SPEI series according to the hydrological year (y-axis). The x-axis represents the different SPEI time scales. The contour plots show the average *r*-values of each derived cluster C_m..... 44

Figure 4.15: Standard deviation of monthly correlations within each cluster C_m. 45

Figure 4.16: Location of the catchments represented by each cluster of the monthly correlation (C_m)..... 47

Figure 4.17: Box plots for mean values of surface area, elevation, slope, rainfall and temperature for those catchments represented by each cluster (C_m) of the monthly correlation analysis. 48

Figure 5.1: Plot of the contingency table for clusters C_m and runoff regimes C_r..... 59

Figure 5.2: Plot of the contingency table for clusters C_m and clusters C_C. 59

List of Tables

Table 3.1: Different states of hydrological conditions based on thresholds of the SSI and corresponding probabilities..... 19

Table 4.1: Percentage of peak *r*-values per SPEI time scale in relation to streamflow conditions..... 32

Abstract

Meteorological drought indicators provide a large range of applications in the field of environmental research. The Standardized Precipitation and Evapotranspiration Index (SPEI) features a multi-temporal character, which can be used to summarize climatic conditions at varying time scales and their effects on different sub-systems of the hydrological cycle. This study investigated the link between the SPEI at temporal scales of 1-12 months and near-natural streamflow patterns. For this purpose, monthly discharge observations of 381 mesoscale catchments in 12 countries across Europe were incorporated. The analysis was carried out for the 1965-2005 period.

To assure accurate spatiotemporal comparability between different hydrological conditions across the study area, the computation of the Standardized Streamflow Index (SSI) was applied. Herein, monthly discharge series were standardized and normalized. The interrelation between different temporal aggregations of climatic conditions and runoff behavior of all incorporated river basins was investigated by performing a correlation analysis between continuous and monthly time series of the SSI and the SPEI at all available time scales. Runoff response to meteorological water balances was furthermore explored as a function of time scales, streamflow conditions and large and small-scale properties of the incorporated catchments. To outline common and distinctive connections between the applied indices and their spatial allocation, cluster analyses were applied.

In general, it was found that both indicators exhibit a high level of interrelation, which is strongly dependent on current streamflow conditions as well as natural influences like snow and groundwater. The cluster analysis provided three major types of continuous streamflow responses: (i) fast reacting river basins; (ii) catchments that tend to intermediate response times; and (iii) river networks with a high degree of “hydrological memory”. In contrast to the interrelation between the continuous series of the SSI and the SPEI, the monthly correlation analysis gave a more detailed and spatial coherent picture of seasonal relations between meteorological conditions and runoff behavior. Seasonal differences between the patterns of linkage reflect Europe’s environmental diversity and illustrate the common influence of snow hydrology and groundwater interaction on streamflow responses to climatic conditions at different time scales.

Keywords:

Drought indicators

Standardized Precipitation Evapotranspiration Index (SPEI)

Standardized Streamflow Index (SSI)

Streamflow patterns

Runoff regimes

Snow

Groundwater

Europe

Zusammenfassung

Meteorologische Dürreindikatoren haben ein breites Anwendungsspektrum in den Umweltwissenschaften. Der Standardized Precipitation and Evapotranspiration Index (SPEI) zeichnet sich durch die Integration mehrerer Zeitskalen aus. Diese ermöglichen es, klimatische Einflüsse auf verschiedene Teile des Wasserkreislaufs zusammenzufassen. Diese Arbeit behandelt den Zusammenhang zwischen dem SPEI in Zeitskalen von 1-12 Monaten und Abflüssen von 381 naturnahen und mesoskaligen Einzugsgebieten in 12 Ländern Europas über den Zeitraum von 1965 bis 2005.

Zum Zweck einer besseren Vergleichbarkeit zwischen den unterschiedlichen Abflussregimen der analysierten Einzugsgebiete wurden die monatlichen Abflusszeitreihen durch die Berechnung des Standardized Streamflow Index (SSI) standardisiert und normalisiert. Der Zusammenhang zwischen verschiedenen Zeitskalen der klimatischen Einflussgrößen und dem Abflussverhalten der Einzugsgebiete wurde mittels Korrelationsanalyse untersucht. Die Abflussreaktion als Folge der meteorologischen Wasserbilanz wurde in Abhängigkeit unterschiedlicher zeitlicher Aggregationen, hydrologischer Schwellwerte sowie groß- und kleinräumiger Eigenschaften der jeweiligen Einzugsgebiete analysiert. Um die untersuchten Relationen in einen übergeordneten Kontext zu stellen, wurden verschieden Clustertechniken verwendet.

Die Ergebnisse zeigen ein generell hohes Maß an Korrelation zwischen den untersuchten Indikatoren. Diese ist in weiten Teilen abhängig von den jeweiligen Abflussbedingungen und anderen natürlichen Einflussgrößen, insbesondere von Schnee und Grundwasser. Die Ergebnisse der Clusteranalyse zeigen, dass zwischen eher schnell und eher langsam reagierenden Einzugsgebieten unterschieden werden kann. Eine weitere Gruppe an naturnahen Flüssen zeichnet sich durch mittelfristige Abflussreaktionen auf meteorlogische Einflussfaktoren aus. Im Gegensatz zur Auswertung der kontinuierlichen Zeitreihen beider Indikatoren, liefert die Korrelationsanalyse zwischen den monatlichen Werten des SSI und des SPEI präzisere und räumlich homogene Resultate. Die saisonalen Muster des Zusammenhangs beider Indikatoren spiegeln die große naturräumliche Heterogenität Europas wieder. Darüber hinaus können der übergeordnete Einfluss von Schneeakkumulations- und Schmelzprozessen sowie von hydrogeologischen Charakteristika auf Abflussreaktionen veranschaulicht werden.

1 Introduction

1.1 Background

1.1.1 Meteorological drought indicators

Drought, as one of the most devastating natural hazards, is a complex phenomenon affecting large areas of both, societal and environmental sectors. Mostly related to a reduced amount of precipitation over a specific time scale and spatial extent, drought causes severe damage to e.g. agriculture and water supplies as well as terrestrial and freshwater ecosystems (MISHRA & SINGH, 2010). Due to the interdisciplinary and many-faceted character of drought, a wide range of definitions and classifications has been set up, each giving respect to either its environmental properties or its particular impact. WILHITE & GLANTZ (1985) classified the phenomenon into meteorological, hydrological, agricultural and socio-economic drought. Beside the categorization of single drought variables, a large variety of drought indicators exist. This multitude of general or specified indices comes due to the fact that drought is of multiscalar nature and therefore needs to be assessed dependently from the different categories, impacted sectors and respective time scales (KEYANTASH & DRACUP, 2002; MISHRA & SINGH, 2010; VICENTE-SERRANO ET AL., 2009; VAN LOON, 2013). As meteorological drought most often precedes other kinds of water shortages, several stochastic or physically based meteorological drought indicators have yet been developed to characterize precipitation deficits in terms of their duration, intensity, magnitude and spatial extent:

Among the first tools to monitor drought characteristics was the Palmer Drought Severity Index (PDSI; PALMER, 1965). The PDSI uses a two-layer soil model to quantify regional water budgets based on precipitation, temperature and soil moisture (KEYANTASH & DRACUP, 2002; VICENTE-SERRANO ET AL., 2012b). The Rainfall Anomaly Index (RAI; VAN ROY, 1965) includes a ranking procedure to calculate positive and negative anomalies of precipitation to define meteorological dry spells. A decile-based monitoring system of climatic droughts was introduced by GIBBS & MAHER (1967). Herein, 3-month totals of rainfall observations are grouped into deciles and meteorological drought states can be derived from the comparison of preceding precipitation sums to the complete ranked time series of rainfall observations. Each of these three indices has its

specific usefulness and shortcomings, but all have in common a more or less pronounced degree of either temporal or regional incomparability. Additionally, these indices due not consider the multi-scalar temporal character of dry spells (GUTTMAN, 1998; KEYANTASH & DRACUP, 2002; CANCELLIERE ET AL., 2007; MISHRA & SINGH, 2010).

The Standardized Precipitation Index (SPI) was developed for drought management in terms of the detection and quantification of drought (MCKEE, 1993) and is one of the most frequently used indices for operational and scientific drought monitoring (CANCELLIERE ET AL., 2007; MISHRA & SINGH, 2010). The SPI is a dimensionless indicator exclusively based on rainfall measurements and therefore not data intensive. Long-term precipitation data is transformed to standardized units regarding to a theoretical distribution function. Normalization is hereby achieved by transforming the fitted probability function to a normal distribution and derived normal standard quantiles of corresponding non-exceedance probabilities represent the resulting SPI values. This is a precondition for comparability between different regions and climatic regimes (KEYANTASH & DRACUP, 2002; CANCELLIERE ET AL., 2007 ; MISHRA & SINGH, 2010). Beside this advantage, the calculation of the SPI can be applied for different time scales with respect to diverse temporal dimensions of water availability in different parts of the hydrological cycle as well as in various sectors of water usage and management (MCKEE, 1993; GUTTMAN, 1998). Therefore the calculation procedure can also be used for precipitation time series of aggregated time scales and is thus capable of defining different aspects and impacts of meteorological drought. Short-term fluctuations of water availability are relevant for soil moisture, whereas hydrological drought can be detected when precipitation deficits are accumulated over longer periods (MCKEE, 1993). In spite of its simplicity, the SPI facilitates a functional definition and universal classification of drought events related to their intensity, severity, as well as their temporal properties.

A recently developed modification of the SPI is the Standardized Precipitation Evaporation Index (SPEI; VICENTE-SERRANO ET AL., 2009). The main intention to develop this indicator was based on the critical issue that the SPI solely relies on precipitation, even though evapotranspiration has to be considered as an important parameter influencing hydro-meteorological water fluxes and resulting moisture conditions. As the variability of evapotranspiration rates is highly dependent on temperature fluctuations, the SPEI is also sensitive to the effects of global warming on the amount of freshwater resources. The computation of the SPEI is carried out in the same way as for the SPI,

whereat a simple monthly water balance (the difference between precipitation and potential evapotranspiration) is used as an input value instead of monthly rainfall aggregations. Hence, the SPEI combines the multi-scalar character of the SPI and is capable of comparing positive and negative climatic anomalies independently from seasons and regions.

1.1.2 Controlling factors on streamflow generation

For natural hydrological systems, precipitation is normally considered as the origin of river discharge (MORIN ET AL., 2009). Nevertheless, runoff and streamflow patterns are additionally dependent on the physical attributes of the respective catchments. Most influencing physiographic properties in terms of hydrological processes within a river basin are its geology, topography, soils and vegetation (SOULSBY ET AL., 2006). Storage, transfer and residence time of water on the catchment-scale is therefore strongly dependent on large and small-scale characteristics (POST & JAKEMAN, 1996). In near-natural catchments, river discharge can be seen as a combined and undisturbed reaction to climatological signals like precipitation and evapotranspiration as well as a function of fluxes and storage of water within the different hydrological subsystems. These include snow cover, soil moisture and groundwater (LÓPEZ-MORENO ET AL., 2013). The temporal aspects of water propagation from precipitation to river runoff have been subject of a variety of investigations. Recent studies highlighted the influence of geology, soil hydrology, topography and meteorological factors on transit times of water (MCDONNELL ET AL., 2010). As transfer times between and within each part of the hydrological water cycle are associated with different time scales, the catchment response to preceding meteorological conditions exhibits a large geographical as well as seasonal heterogeneity (LÓPEZ-MORENO ET AL., 2013). The latter characteristic comes also due to the importance of snow for the hydrological cycle, which has a strong influence on seasonal reactions of river discharge to precipitation conditions (SOULSBY ET AL., 2006; MCDONNELL ET AL., 2010). Additionally, regional investigations confirmed the effects of seasonal soil moisture and precipitation conditions on runoff responses (GARCÍA-RUIZ ET AL., 2008; LATRON & GALLART, 2008).

1.1.3 Linking meteorological drought indicators with hydrological variables

Previous efforts have been made to characterize and quantify the explanatory power of meteorological drought indices relating to water availability in different parts of the terrestrial water cycle. Nevertheless, research so far mostly focused on the linkage between meteorological drought indicators and hydrological dry spells, in accordance to their originally intended field of application. SZALAI ET AL. (2000) analyzed spatial and temporal heterogeneities among the relationship between the SPI at a variety of time scales and different types of surface water resources like river discharges and reservoir storages in Hungary. ZAIDMAN ET AL. (2001) studied spatiotemporal aspects of the relationship between streamflow depletion and meteorological drought. Drought development and propagation in north-west Europe were investigated by comparing regional rainfall and streamflow anomalies for the 1960-1995 period and for historical drought events in Europe. VICENTE-SERRANO & LÓPEZ-MORENO (2005) investigated the usefulness of different time scales of the SPI to explain spatiotemporal variations of usable water resources in the form of river discharges and reservoir storages in a mountainous basin in the Spanish Central Pyrenees. A computational approach to forecast hydrological drought was set up by NALBANTIS & TSAKIRIS (2008). They developed a standardized streamflow index (Streamflow Drought Index; SDI) and used time series of the SPI to derive a linear function of the meteorological indicator which can be applied to predict streamflow drought in the absence of hydrological data. VASILIADES & LOUKAS (2009) applied a correlation analysis between normalized and standardized variables of climatic and hydrological variables to assess their interrelation during drought events in Thessaly, Greece. LORENZO-LACRUZ ET AL. (2010) illustrated the effect of evaporation on the linkage between different hydrological systems and meteorological drought. They correlated time series of the SPI and the SPEI to standardized values of river discharge and reservoir storage in the headwaters of the Tagus River in central Spain. ZHAI ET AL. (2010) carried out a regional study in the territory of China to assess the usefulness of meteorological drought indices for streamflow characterization. They correlated the PDSI and SPI with runoff anomalies to describe long-term runoff variations and trends as a function of precipitation conditions. A study in several sub-catchments of the highly regulated Ebro basin in Spain proved the effects of catchment characteristics on the most accurate SPEI time scale for the characterization of hydrological processes in different subsystems of the terrestrial water cycle (LÓPEZ-MORENO ET AL., 2013).

1.2 Motivation and Objectives

Even though a multitude of studies have investigated the link between several meteorological drought indicators and hydrological variables of interest, most of these investigations concentrated on drought propagation from precipitation deficits to hydrological drought. Nevertheless, standardized and normalized drought indicators like the SPI and the SPEI have the potential to describe and quantify not only climatic drought spells but also meteorological conditions which are characterized by a large degree of water availability. Beside this universal applicability, the SPEI carries multiscalar information about moisture conditions, as it can be computed at different time scales. Hence, the interrelations between climatic variabilities and different subsystems of the terrestrial water cycle can be characterized independently and therefore used to explain streamflow reactions to meteorological conditions in a more detailed way. Additionally, little is known about the validity of these indices concerning spatiotemporal streamflow patterns at the pan-European scale. Given Europe's environmental diversity, standardized and normalized drought indicators are also capable of a spatiotemporal comparison between catchments situated across large parts of the continent. The first objective of this study is the computation of a streamflow indicator for an accurate spatial and temporal comparison of streamflow patterns between all incorporated catchments. The linkage between meteorological drought indicators and streamflow patterns is investigated in two ways:

Firstly, the interrelation between standardized and normalized indicators of climatic conditions and streamflow patterns is investigated dependent on

- different temporal aggregations of the meteorological water balance and
- various streamflow conditions as well as
- the runoff regime of the respective catchment.

Secondly, the response of all incorporated catchments is analyzed not only as function of varying time scales but also as a function of seasonal variations of both meteorological as well as hydrological conditions.

These methodological approaches are applied to elucidate the strength of the link and the respective climatic time scale as well as to detect regional differences and similarities among the included river basins.

2 Data and study area

2.1 Drought indices

2.1.1 Initial dataset

The Standardized Precipitation Evaporation Index was provided by the Drought-R&SPI project as monthly layered raster dataset stretching over Europe with a spatial resolution of 0.25° for each cell. The dataset covers the period from 1950 to 2012 and is available in form of different temporal aggregations from 1 to 12 months.

The meteorological drought indicator is standardized for the 1971-2000 reference period, using the generalized extreme value distribution. The incorporated values of potential evapotranspiration are estimated by applying Hargreaves' method.

2.1.2 Time series computation of the SPEI

Time series of all available SPEI time scales were generated for each catchment by calculating the areal percentages of each intersecting cell within the corresponding basin boundaries. Based on the relative spatial proportion, SPEI values were extracted for each time step of the respective raster layer and finally assembled over the whole period of investigation.

Because of spatial disparities between the geographical extends of available catchment geodata and maps of the SPEI, several catchments with missing indicator values had to be deleted from the dataset.

2.2 Discharge data

2.2.1 Runoff time series of near-natural and mesoscale catchments

Initial streamflow data was collected by the FRIEND (Flow Regimes from International Experiment and Network Data) project, an initiative under UNESCO's International Hydrological Programme (IHP). Its hydrological database, the European Water Archive (EWA), contains long-term daily flow data and catchment information of about 3800

river gauging stations in 29 countries and is hosted by the Global Runoff Data Center (GRDC).

As a part of the EU WATCH (Water and Global Change) project, STAHL ET AL. (2010) updated the existing database in the course of their assessment of streamflow trends in Europe. Actualization and collection of new streamflow records were made based on different criteria: Amongst others, only gauging data of small catchments (areas must not exceed 1000 km^2) was incorporated, which exhibited homogenous daily runoff measurements of high quality with a temporal span of at least 40 years and until the year 2004. Additional stations, included in the final catchment database, are situated in France, Spain, Slovakia and the Baltics.

For this study, a regional subset of 762 near-natural and mesoscale basins across Europe was used to ensure the absence of anthropogenic influences. The dataset contains mean daily discharge observations [m^3 sec^{-1}] and additional geographical information (country, region, gauging station, river name, longitude and latitude and basin area for each of the included basins). Furthermore, available time series were divided up according to their quality. This distinction was made based on the number and type of visible artefacts like constant low or high flows, step functions and data gaps.

2.2.2 Catchment geodata

Catchment boundaries for all observation sites, provided by the EWA, are originally adapted from the second version of the River and Catchment Database for Europe - CCM (VOGT ET AL., 2007), which primarily covers the whole European continent as well as the Atlantic islands, Iceland and the territory of Turkey. It contains an assemblage of rivers and catchments based on the Strahler stream order. Shapefiles, which represent the catchments of the investigated gauging stations, were extracted by the University of Freiburg. They represent each catchment's boundary and a set of statistical values (minimum, maximum, mean and standard deviation) regarding their environmental properties like elevation, slope, precipitation and temperature.

2.2.3 Quality assessment

In the first place, time series of poor quality were deleted from the original dataset. Examination of data gaps and detection of a common time span of all discharge measurements was accomplished by visual screening. Time series with data gaps longer

than 10% of their total length were removed. Gap filling of data series with a maximum of 10% missing values was done by using linear regression analysis. For this purpose, flow records of adjacent gauging stations were incorporated as independent variables. Only series with a resulting Pearson's correlation coefficient of at least r = 0.8 were retained in the data set.

All available time series of good quality were finally aggregated from mean daily discharges to mean monthly streamflow values according to the given minimum time scale of the utilized SPEI data series.

The resulting time series of streamflow observations and the meteorological indicator cover the period from 1965 to 2005. After the quality assessment, 381 catchments are finally incorporated in this study. They are situated in the territories of Austria (44), the Czech Republic (12), Germany (128), Denmark (14), Finland (5), France (58), Norway (35), Sweden (7), Switzerland (19), Slovakia (16), Spain (10) and the UK (33). The entire area, including the catchments, has a south-north extension from the mountain range of the Iberian System in Spain to the Norway-Russian border, which also marks the eastern boundary. The westernmost catchments are located in the Cantabrian Mountains as well as along the western regions of the UK. The analyzed river basins are spatially distributed across a wide range of different natural environments. This fact implies the large heterogeneity among all catchments in relation to their discharge-relevant characteristics. These are going to be summarized in the course of the following analyses.

3 Methods

3.1 Computation of the Standardized Streamflow Index

To discover the linkage between the SPEI and streamflow across Europe, an index has to be computed which exhibits contrastable properties. Therefore the Standardized Streamflow Index (SSI; VICENTE-SERRANO ET AL., 2011) is adopted for this study. The SSI transforms runoff time series to standardized *z*-scores and therefore enables comparisons between streamflow records across space and time, as it is not sensitive to hydrological regimes and total runoff magnitudes. This depicts an indispensable requirement for a consistent evaluation of catchments distributed throughout large parts of the European continent.

3.1.1 Implementation of different distributions functions

Time series of hydrological observations generally exhibit a biased and skewed distribution and therefore do not follow the Gaussian function (LORENZO-LACRUZ ET AL., 2010). A large set of different probability distributions has yet been tested and applied for the computation of various indicators to quantify hydrological drought following the approach of standardization (VICENTE-SERRANO ET AL., 2012b).

In opposition to climatic variables like precipitation and evapotranspiration, river runoff is characterized by a high spatial heterogeneity (LÓPEZ-MORENO ET AL., 2012). This variability is reflected in the variety of different distribution functions used to obtain standardized indicators for streamflow variations in different regions:

For the examination of spatiotemporal aspects of streamflow droughts in north-west Europe, ZAIDMAN (2001) fitted the log-normal distribution to time series of daily discharge measurements. The same probability function was applied by NALBANTIS & TSAKIRIS (2009) for the development of the Streamflow Drought Index (SDI) and its application in the Evinos catchment, Greece. SHUKLA & WOOD (2008) selected the 2-parameter gamma and log-normal distributions to compute the Standardized Runoff Index (SRI) for drought monitoring across the United States. A regional study in Central Spain applied the Pearson type III distribution as well as the log-normal distribution to assess drought impacts on different hydrological systems (LORENZO-LACRUZ ET AL., 2010).

This illustrates that the calculation of standardized time series is highly sensitive to the chosen distribution function and may lead to errors in the estimation of extreme percentiles and respective values of the particular streamflow indicator (VIDAL ET AL., 2010; SHUKLA & WOOD, 2008; VICENTE-SERRANO ET AL., 2011).

In consideration of this potential error source, the methodology of VICENTE-SERRANO (2011) was applied in the course of this study. For the computation of the Standardized Streamflow Index (SSI), this methodological approach incorporates a selection of theoretical probability functions: the Generalized Extreme Value, Person type III, log-logistic, lognormal, Generalized Pareto and Weibull distributions. All have in common broad and longstanding implementations in hydrological sciences (CHOW ET AL., 1988) and allow accurate adaptation to the empirical distribution due to their wide range of statistical values and corresponding distributional shapes.

3.1.1.1 Generalized Extreme Value distribution

The cumulative distribution function of the Generalized Extreme Value distribution can be calculated with the following equation:

$$F(x) = e^{-\left[1-\kappa\left(\frac{x-\mu}{\alpha}\right)\right]^{\frac{1}{\kappa}}} \tag{3.1}$$

Required parameters are derived from the formula developed by HOSKING ET AL. (1985):

$$\kappa = 7.859C + 2.9554C^2 \tag{3.2}$$

$$C = \frac{2}{3+\tau_3} - 0.6309 \tag{3.3}$$

$$\alpha = \frac{\lambda_2 \kappa}{\Gamma(1+\kappa)(1-2^{-\kappa})} \tag{3.4}$$

$$\mu = \lambda_1 + \frac{\alpha}{\kappa}[\Gamma(1+\kappa) - 1] \tag{3.5}$$

3.1.1.2 Pearson type III distribution

Relating to the Pearson III distribution, the probability distribution function of x (data of the specific monthly discharge series) can be calculated as follows:

$$F(x) = \frac{1}{\alpha\Gamma(\beta)} \int_{\gamma}^{x} \left(\frac{x-\gamma}{\alpha}\right)^{\beta-1} e^{-\left(\frac{x-\gamma}{\alpha}\right)} \tag{3.6}$$

Parameters of the Pearson III distribution function can be derived by the approach of HOSKING (1990):

If $\tau_3 \geq 1/3$ then $\tau_m = 1 - \tau_3$, and β can be calculated such as:

$$\beta = \frac{(0.36067\tau_m - 0.5967\tau_m^2 + 0.25361\tau_m^3)}{(1 - 2.78861\tau_m + 2.56096\tau_m^2 - 0.77045\tau_m^3)} \tag{3.7}$$

If $\tau_3 < 1/3$ then $\tau_m = 3\pi\ \tau_3^2$, and β can be obtained using the expression:

$$\beta = \frac{(1 + 0.2906\tau_m)}{(\tau_m + 0.1882{\tau^2}_m + 0.0442{\tau^3}_m)} \tag{3.8}$$

$$\alpha = \sqrt{\pi}\lambda_2 \frac{\Gamma(\beta)}{\Gamma\left(\beta + \frac{1}{2}\right)} \tag{3.9}$$

$$\gamma = \lambda_1 - \alpha\beta \tag{3.10}$$

3.1.1.3 Log-logistic distribution

The cumulative distribution function of the log-logistic distribution is calculated applying the expression of SINGH ET AL. (1993):

$$F(x) = \left[1 + \left(\frac{\alpha}{x-\gamma}\right)^{\beta}\right]^{-1} \tag{3.11}$$

The Below-mentioned terms return the parameters for the computation of the log-logistic distribution:

$$\beta = \frac{2w_1 - w_0}{6w_1 - w_0 - 6w_2} \tag{3.12}$$

$$\alpha = \frac{(w_0 - 2w_1)\beta}{\Gamma\left(1 + \frac{1}{\beta}\right)\Gamma\left(1 - \frac{1}{\beta}\right)} \tag{3.13}$$

$$\gamma = w_0 - \alpha\Gamma\left(1 + \frac{1}{\beta}\right)\Gamma\left(1 - \frac{1}{\beta}\right) \tag{3.14}$$

3.1.1.4 Weibull distribution

The cumulative distribution function of the Weibull distribution is obtained following the formula of HOSKING (1986):

$$F(x) = 1 - e^{-\left(\frac{x-m}{\alpha}\right)^b} \tag{3.15}$$

where the required parameters can be assessed as:

$$b = \frac{1}{(7.859C + 2.9554C^2)} \tag{3.16}$$

$$C = \frac{2}{3 - \tau_3} - 0.6309 \tag{3.17}$$

$$\alpha = \frac{\lambda_2}{\Gamma\left(1 + \frac{1}{b}\right)\left(1 - 2^{-\frac{1}{b}}\right)} \tag{3.18}$$

$$m = \lambda_1 - a\Gamma\left(1 + \frac{1}{b}\right) \tag{3.19}$$

3.1.1.5 Lognormal distribution

The cumulative distribution function of the lognormal distribution is calculated as:

$$F(x) = \Phi\left(\frac{ln(x - a) - \mu}{\sigma}\right) \tag{3.20}$$

Where Φ is the standard normal cumulative distribution function. Parameters can be obtained using the following expressions according to HOSKING (1990):

$$\sigma = 0.999281z - 0.006118z^2 + 0.000127z^5 \tag{3.21}$$

$$z = \sqrt{\frac{8}{3}}\Phi^{-1}\left(\frac{1+\tau_3}{2}\right) \tag{3.22}$$

$$\mu = ln\left[\frac{\lambda_2}{erf\left(\frac{\sigma}{2}\right)}\right] - \frac{\sigma^2}{2} \tag{3.23}$$

The Gauss error *erf* function can be obtained using the formula:

$$erf\left(\frac{\sigma}{2}\right) = 2\Phi\left(\frac{\sigma}{2}\sqrt{2}\right) - 1 \tag{3.24}$$

$$a = \lambda_1 - e^{\mu+\frac{\sigma^2}{2}} \tag{3.25}$$

3.1.1.6 Generalized Pareto distribution

The probability distribution function of the Generalized Pareto distribution is given by:

$$F(x) = 1 - \left[1 - \frac{\kappa}{\alpha}(x-\varepsilon)\right]^{\frac{1}{\kappa}} \tag{3.26}$$

Required parameters are derived according to HOSKING (1990):

$$\kappa = \frac{(1-3\tau_3)}{1+\tau_3} \tag{3.27}$$

$$\alpha = \lambda_2(1+\kappa)(1+\kappa) \tag{3.28}$$

$$\varepsilon = \lambda_1 - \lambda_2(2+\kappa) \tag{3.29}$$

3.1.2 Parameter estimation based on L-Moments

To obtain the cumulative distribution functions $F_{(x)}$ for each of the six distributions, parameters were calculated based on the method of L-moments (HOSKING, 1990). L-coefficients of skewness and kurtosis, τ_3 and τ_4 respectively were computed as:

$$\tau_3 = \frac{\lambda_3}{\lambda_2} \tag{3.30}$$

$$\tau_4 = \frac{\lambda_4}{\lambda_2} \tag{3.31}$$

where λ_2, λ_3 and λ_4 are the L-moments of the 12 monthly discharge series of each of the 381 analyzed catchments. These were derived from the probability weighted moments of the empirical runoff data by using the formulae:

$$\lambda_1 = \omega_0 \tag{3.32}$$

$$\lambda_2 = \omega_0 - 2\omega_1 \tag{3.33}$$

$$\lambda_3 = \omega_0 - 6\omega_1 - 6\omega_2 \tag{3.34}$$

$$\lambda_4 = \omega_0 - 12\omega_1 - 30\omega_2 - 20\omega_3 \tag{3.35}$$

To compute the probability weighted moments of order s, the following equation was used:

$$w_s = \frac{1}{N}\sum_{i=1}^{N}(1 - F_i)^s x_i \tag{3.36}$$

where x_i is the monthly value of the particular discharge series and F_i is the frequency estimator, which can be obtained following the approach of HOSKING (1990):

$$F_i = \frac{i - 0.35}{N} \tag{3.37}$$

3.1.3 Conversion to standardized z-scores

Once all cumulative distribution functions are calculated, the SSI for each time step of the original discharge time series can be derived using the approach of classical approximation, which was developed by ABRAMOWITZ & STEGUN (1965):

$$SSI = W - \frac{C_0 + C_1 W + C_2 W^2}{1 + d_1 W + d_2 W^2 + d_3 W^3} \tag{3.38}$$

where:

$$W = \sqrt{-2\ln(P)} \; for \; P \leq 0.5 \tag{3.39}$$

or:

$$W = \sqrt{-2\ln(1-P)} \; for \; P \geq 0.5 \tag{3.40}$$

P is herein the exceedance probability for a specific value of x and is calculated as:

$$P = 1 - F(x) \tag{3.41}$$

It is important to note that the signing of resulting SSI values is reversed for $P \geq 0.5$. The constants are: C_0 = 2.515517, C_1 = 0.802853, C_2 = 0.010328, d_1 = 1.432788, d_2 = 0.189269 and d_3 = 0.001308.

This transformation implies that cumulative probabilities of analyzed discharge values are normalized with a mean of zero and a standard deviation of one. SSI values of zero indicate discharges of 50 % of the accumulated probability according to each of the particular distribution functions (LÓPEZ-MORENO ET AL., 2009).

3.1.4 Goodness-of-fit test: Best Monthly Fit approach

To select the most suitable probability distribution for the computation of an accurate SSI, the Best Monthly Fit approach (BMF; VICENTE-SERRANO ET AL., 2012) is applied. The analyzed discharge time series and their attendant probability distributions are

compared in relation to the respective difference between the empirical distribution and its reference theoretical distribution function. This computational procedure is based on the Kolgomorov-Smirnov test (SIEGEL & CASTELAN, 1988) which is defined by:

H_0: The runoff time series follows the specified theoretical distribution function.

H_a: The runoff time series follows the specified theoretical distribution function.

The resulting test statistic of the Kolgomorov-Smirnov test, here referred to as D-statistic *D*, represents the maximum vertical difference between the compared distributions. It is obtained with the following expression:

$$D = max\left(max_i \left|CDF(x_i) - \frac{r-1}{n}, \frac{r}{n} - CDF(x_i)\right|\right) \quad (3.42)$$

where the rank of the specific observation i in ascending order is described as r, and n is the total number of observations. *CDF(x)* represents the particular cumulative theoretical distribution function of the tested distribution function.

The Kolgomorov-Smirnov test is carried out for each of the six applied distribution functions with a critical value of $\alpha = 0.05$. As D approximates to 0 when the discharge time series follows the tested theoretical distribution function, the one with the smallest D-statistic was chosen to be included in the computation of the respective SSI time series.

3.2 Assessing the linkage between the SPEI and the SSI

3.2.1 Correlation analysis

To assess the general linkage between indicators for meteorological and hydrological conditions, a correlation analysis between the SPEI at different time scales and SSI is performed. This approach is carried out for each of the 381 catchments over the whole period of investigation (1965 - 2005).

To characterize the fundamental association, Pearson's correlation coefficients (r-values) are computed between the time series of the SSI and the SPEI at timescales be-

tween 1 and 12 months to discover temporal variations of the linkage, especially the maximal strength of the link and the respective temporal aggregation.

$$r = \frac{\sum_{i=1}^{n}(x_i -)(y_i - \bar{y})}{\sqrt{\sum_{i=1}^{n}(x_i - \bar{x})^2 \sum_{i=1}^{n}(y_i - \bar{y})^2}} \tag{3.43}$$

where x_i and y_i are the corresponding values of the SPEI and SSI time series and $\bar{x}$ and $\bar{y}$ represent the associated average values of each series. The number of correlated observations is included in the formula as n.

The correlation between time series of the SSI and the SPEI is also investigated as a function of hydrological conditions in each catchment. Herein, only those time steps of both indicators are used in the correlation analysis for which SSI values are within a range of predefined thresholds relating to streamflow conditions defined by NALBANTIS & TSAKIRIS (2009). Different hydrological states, their drought index thresholds and associated probabilities of occurrence are listed in Table 2.1.

Table 3.1: Different states of hydrological conditions based on thresholds of the SSI and corresponding probabilities.

SSI value	Category	Probability (%)
SSI ≥ 0.0	Non-drought	50.0
SSI ≤ 0.0	Drought	50.0
-1.0 ≥ SSI < 0.0	Mild drought	34.1
-1.5 ≥ SSI < -1.0	Moderate drought	9.2
-2.0 ≥ SSI < -1.5	Severe drought	4.4
SSI < -2.0	Extreme drought	2.3

3.2.2 Cluster analysis of the continuous correlations

For the investigation of continuous correlation patterns, series of *r*-values between SSI and SPEI time scales of 1-12 months are grouped by hierarchical clustering. For this purpose, resulting series of *r*-values for all catchments are again correlated to each other.

Hereby, the 12 resulting Pearson's coefficients for each catchment are represented as x_i and y_i (Formula 2.43) and are in turn correlated to each other. The associated average

values $\bar{x}$ and $\bar{y}$ represent the statistical means of each correlation series computed in the first methodological step.

Once the correlation matrix between all observation sites is computed, resulting *r*-values r_i between each catchment are converted to Pearson's distance measures $d_{p,i}$ which can be obtained using the formula:

$$d_{p,i} = 1 - r_i \tag{3.44}$$

and finally classified by hierarchical cluster analysis based on the incremental sum of squares method (RENCHER, 2002). This approach is in principle based on the iteratively combination of clusters as a function of the smallest increase of variance of resulting clusters:

$$D_w(C_j C_k) = \frac{n_j n_k}{n_j + n_k} \left\| \bar{x}_j - \bar{x}_k \right\|^2 \tag{3.45}$$

Dw represents the Ward-distance between two clusters C_j and C_k, whereby $\bar{x}_j$ and $\bar{x}_k$ represent the arithmetic means of all objects n_j and n_k of each cluster. The fundamental principle of this hierarchical agglomerative clustering method is to merge those clusters which cause the smallest increase of variance within the new cluster and therefore generate the minimum loss of heterogeneity inside the new group.

This method is applied, because it produces the most consistent results in terms of heterogeneity between and homogeneity within resulting clusters of continuous linkages between SSI and SPEI values. Selection of the final number of clusters is achieved by visual assessment of the sum of within-cluster distances in relation to the increasing amount of clusters.

3.2.3 Calculation of hydrological regimes

Hydrological regimes characterize the average seasonal streamflow characteristics and can be seen as an integration of the main environmental properties like their physiographic and climatic conditions (KRASOVSKAIA ET AL., 1994). Hence, they are incorporated in the analysis of temporal and regional patterns of the linkage between the SSI and the SPEI.

Hydrological regimes are determined by annual series of monthly Pardé-coefficients (PARDÉ, 1934), which can be calculated as follows:

$$PC_{m(i)} = \frac{\bar{Q}_{m(i)}}{\bar{Q}_a} \tag{3.46}$$

$PC_{m(i)}$ represents the Pardé-coefficient of the specific month, $\bar{Q}_m$ is the average runoff [m³ seq^{-1}] of month i over all years of observation and $\bar{Q}_a$ is the annual mean discharge [m³ seq^{-1}]. Resulting series of Pardé-coefficients are normalized and dimensionless and therefore exhibit a mean of 1 and can be used for interregional comparisons of discharge distributions, independently of river flow magnitudes.

After the computation of all monthly Pardé-coefficients, resulting data series of all catchments are clustered to obtain relatively homogenous hydrological regimes across Europe. In contrast to the classification of linkages between continuous SSI and multi-scale SPEI series, a non-hierarchical clustering approach is applied. Hereby, most consistent streamflow regimes are obtained by the *k*-means clustering method, which is an algorithm based on the minimization of the sum of squares within iteratively reduced amounts of initial clusters (RENCHER, 2002). The target function to be optimized is expressed as:

$$min \sum_{j=1}^{k} \sum_{i=1}^{n} \left\| x_{i,j} - c_j \right\|^2 \tag{3.47}$$

where $x_{i,j}$ represents the datapoint consisting of 12 monthly Pardé-coefficients and c_j represents the centroid of characteristic values within one of the particular clusters k. The number of datapoints to be clustered is incorporated as n and corresponds to all 381 analyzed catchments.

The algorithm classifies clusters according to the Euclidian distance from initial, randomly chosen cluster centers of a predefined number. Then it iteratively redefines cluster centers as the averages of the cases in the latest cluster, until cases no longer change membership between clusters.

As variables to be clustered, Pardé-coefficients exhibit common scales with a theoretical minimum of 0 and possible extreme values of 12 and therefore do not need to be

standardized in preparation of the *k*-means clustering algorithm which is not scale-invariant.

3.2.4 Correlation and cluster analysis of the monthly SPEI and SSI series

In addition to the correlations of the continuous time series, monthly series are derived from both indicators resulting in 12 independent series (January - December) with 40 time steps (1965 - 2005). This set of series is obtained for each basin in case of the SSI and corresponding series for each time scale of the SPEI. All monthly series are ordered according to the hydrological year (October - September).

For all drainage basins, Pearson's correlation coefficients are again calculated between monthly series of the SSI and the SPEI at each time scale. This approach is applied to obtain the influence of seasonality and temporal aggregation on the quantitative degree of correlation between the two indices.

Resulting matrices of *r*-values, as functions of season and time scale are, subsequently clustered following the same agglomerative approach as for the series of *r*-values between the continuous SSI and SPEI values. For this purpose a correlation matrix between the resulting matrices of all catchments is computed and obtained correlation coefficients are again converted to Pearson's distance measures and finally clustered using Ward's Method.

4 Results

4.1 Overall relationship between the SSI and the SPEI

Figure 3.1 demonstrates the results of the correlation analysis between the continuous times series of the SSI and the SPEI. The resulting correlation coefficients are firstly grouped according to the different temporal aggregations of the SPEI and secondly as a function of streamflow conditions. Hereby the correlation was applied for those values of both indicators, during which the SSI was within predefined threshold levels, as illustrated in Table 2.1.

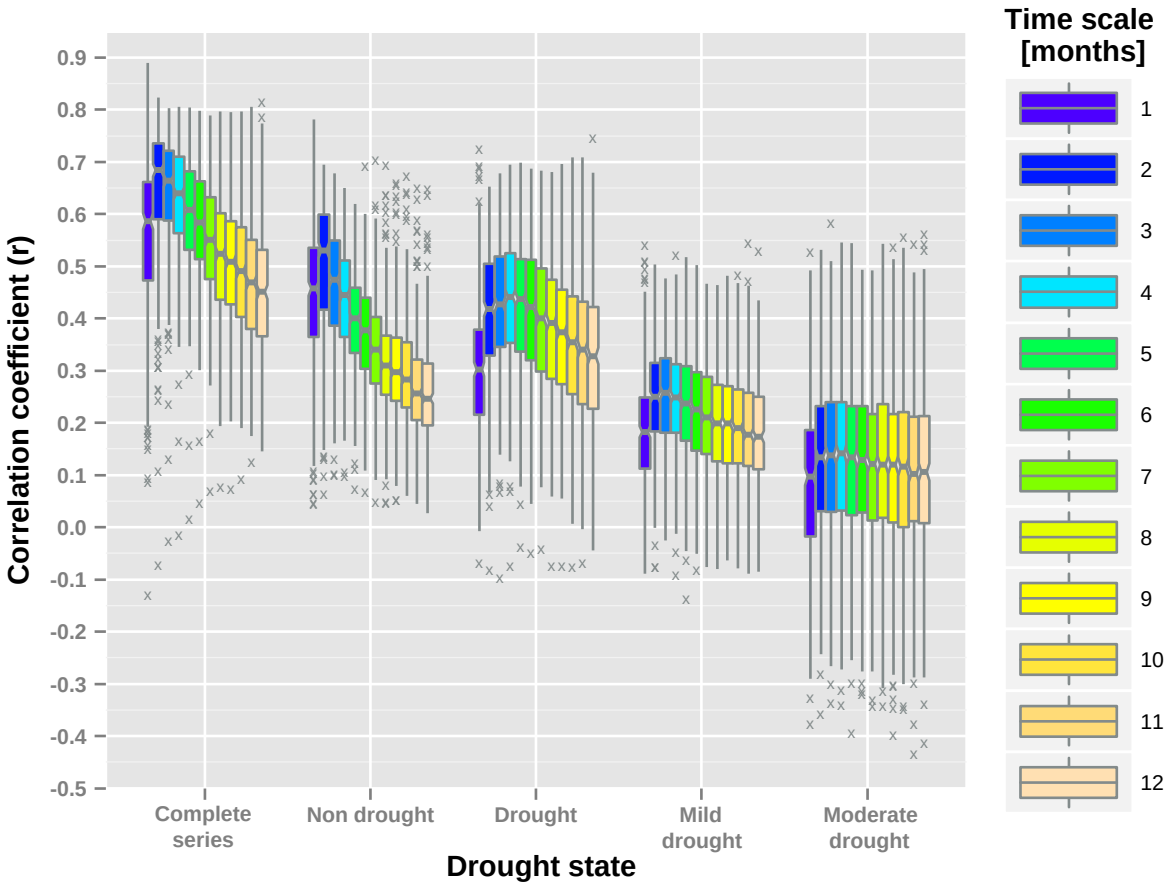

Figure 4.1: Correlations between continuous series of the SSI and the SPEI at different time scales in relation to different streamflow conditions.

The analysis conducted over the whole period of investigation shows a maximum of correlation for a SPEI time scale of 2 months with respect to the first, second and third

quartile. As the time scales increase the overall linkages between the continuous series exhibit a constant decrease of correlations to their minimum at a time scale of 12 months. The linkage of both indicators during non-drought periods exhibits a similar course of statistical values with rapidly declining correlations from smaller to longer time scales of the meteorological drought index. In contrast, the development of correlation coefficients for periods of hydrological drought is characterized by a sharp rise from monthly SPEI values to temporal aggregations of 2 months and a further increase of correspondence culminating at a SPEI time scale of 4 months. For larger scales, the coefficients indicate decreasing relationships between both indicators. For mild streamflow drought events, the displayed quartiles of *r*-values exhibit a balanced distribution with a maximum at a SPEI scale of 3 months and a rather slight decrease towards larger scales. This progression is also applicable for moderate runoff drought conditions but exhibits no clear peak and an even more balanced course of quartiles. Comparison of the general linkages between both indicators elucidates overall differences between the hydrological drought states. Indicators for climatic and hydrological conditions show the highest levels of correlation for the complete time series, whereas a continuous drop of overall correlations can be seen with increasing drought intensities. When comparing the opposing states drought and non-drought, defined by SSI values below or above 0, a characteristic feature is that both series indicate similar levels of overall correlation. Nevertheless, correlations for shorter time scales are of higher rank during non-drought periods, whereas discharge and climatic indicators move towards higher levels of synchronicity for intermediate and longer time scales of the SPEI in the time of hydrological drought. For SPEI time scales between 5 and 12 months correlations during drought periods are superior to those of wet conditions. All drought states have in common a similar course of correlation statistics between SPEI time scales of 1 and 2 months, which becomes apparent from sharp increases of interrelation between these two scales. Correlation coefficients obtained for severe and extreme hydrological drought conditions are ignored in the assessment of the linkage between SSI and SPEI time series. This comes due to insufficient amount of time steps within or below the corresponding threshold levels and thus to a lack of significant correlations of incorporated catchments.

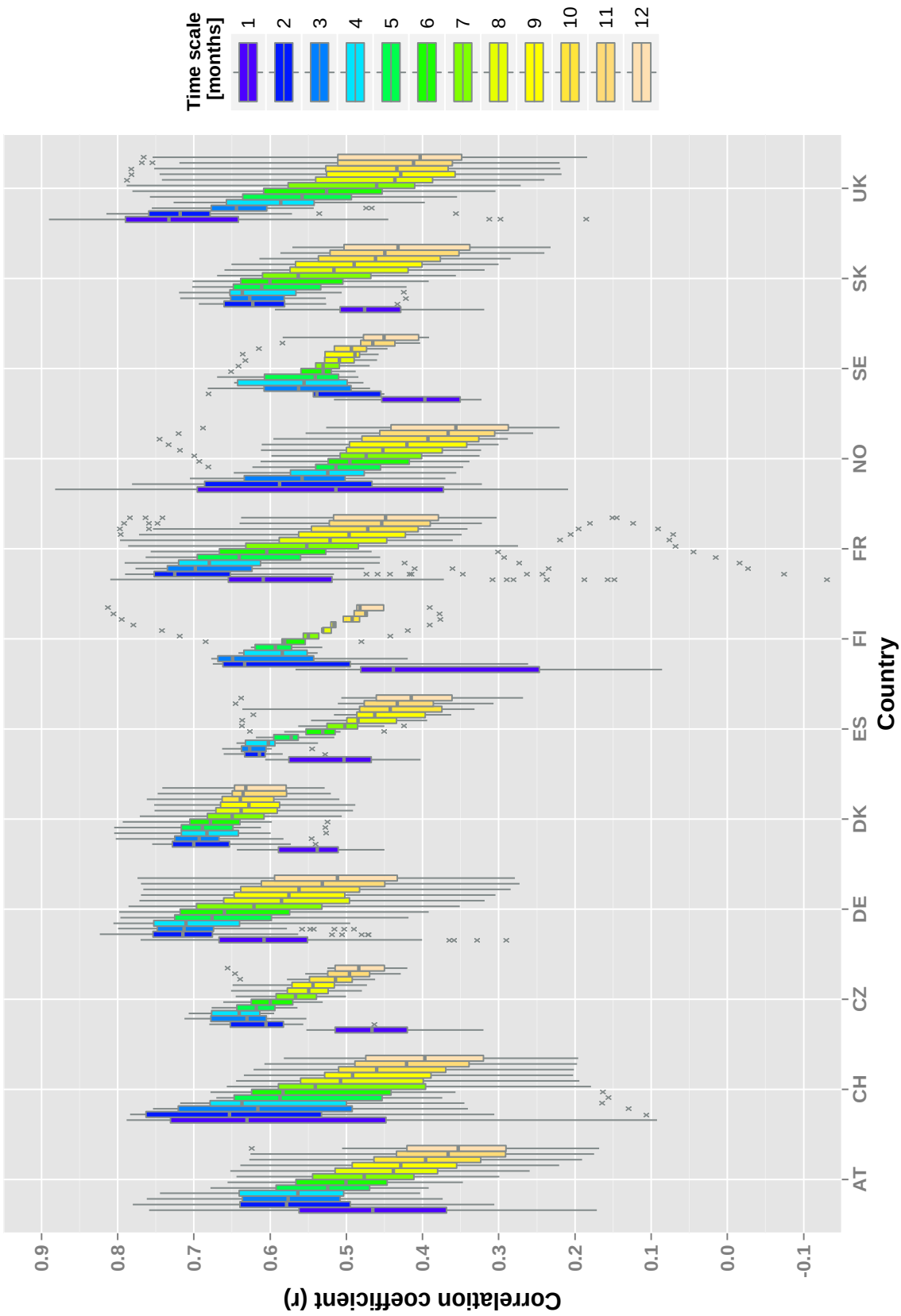

Figure 4.2: Box plots of correlations between continuous series of the SSI and the SPEI at different time scales for each country.

The connection between the complete continuous series of both indicators according to the countries involved in this study is visualized in Figure 3.2. Despite the high level of intra- and inter-group variance of statistical values, some broad common as well as differing features can be obtained. Courses of scale dependent quartiles show an increase of relationship from the monthly SPEI to a time scale of 2 months for all countries with the exception of the United Kingdom. The latter time scale represents the peak of median correlation coefficients for all countries besides the UK (1 month), Spain, Finland and Spain (3 months), as well as the Czech Republic and Slovakia (4 months). Additionally, all countries exhibit decreasing quartiles of correlation with ascending scales of the standardized climatic water balances. In contrast, catchments in the Czech Republic, Denmark, Finland and Sweden tend to have lowest correlations at the shortest time scale of the SPEI. Highest medians of *r*-values can be observed in Germany, France and Denmark whose catchments generally exhibit high levels of correspondence at SPEI time scales between 2 and 12 months. Lowest overall correlations can be found for rivers in Austria and Sweden. The descriptive correlation statistics reveal striking outliers in the cases of Finland and France. For Finland, the remarkable anomalies of correlations most likely occur due to the small number of incorporated river basins. The latter country includes several exceptionally low coefficients of correlation approaching to negative *r*-values.

4.2 Maximum correlation per catchment

Table 3.1 summarizes the highest explanatory power of all SPEI time scales applied in the correlation analysis. Strongest correlations are most numerous for SPEI time scales of 2 months in cases of the complete series, non-drought periods and events of mild and moderate drought. The amount of maximum *r*-values is furthermore characterized by a sharp drop of peak correlations towards higher time scales for the complete time series and non-drought events. In contrast, peak correlations of most catchments are more evenly distributed among the varying time scales of the SPEI for the several hydrological drought spells. For drought in general, most catchments show the greatest linkage when the SSI is correlated to a SPEI of 4 months, but there are also numerous catchments with a high level of similarity between both indicators at SPEI time scales of 2 months.

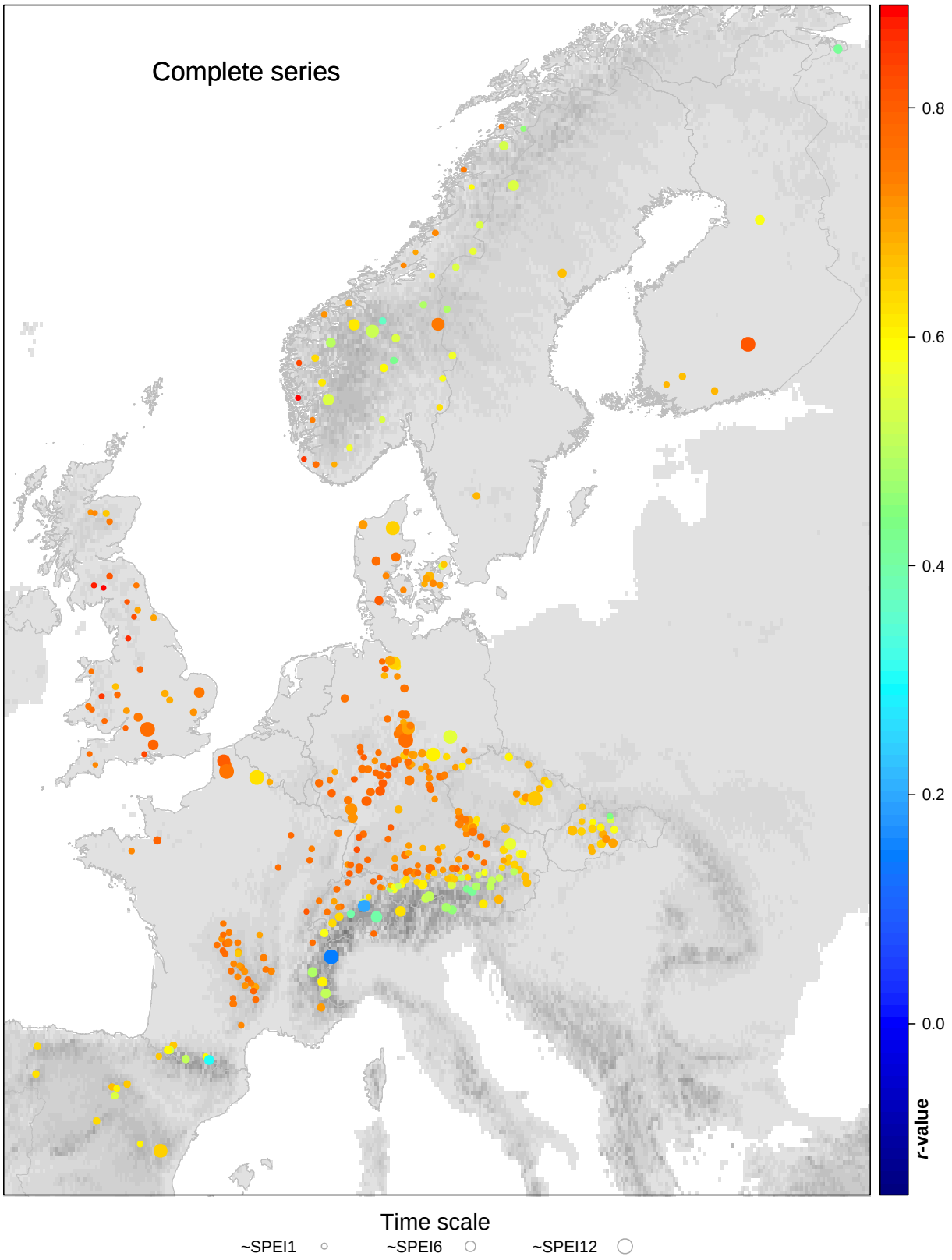

Figure 4.3: Maximum strength of the correlation between both indicators and the respective SPEI time scales (1-12 months) for the complete period of observation.

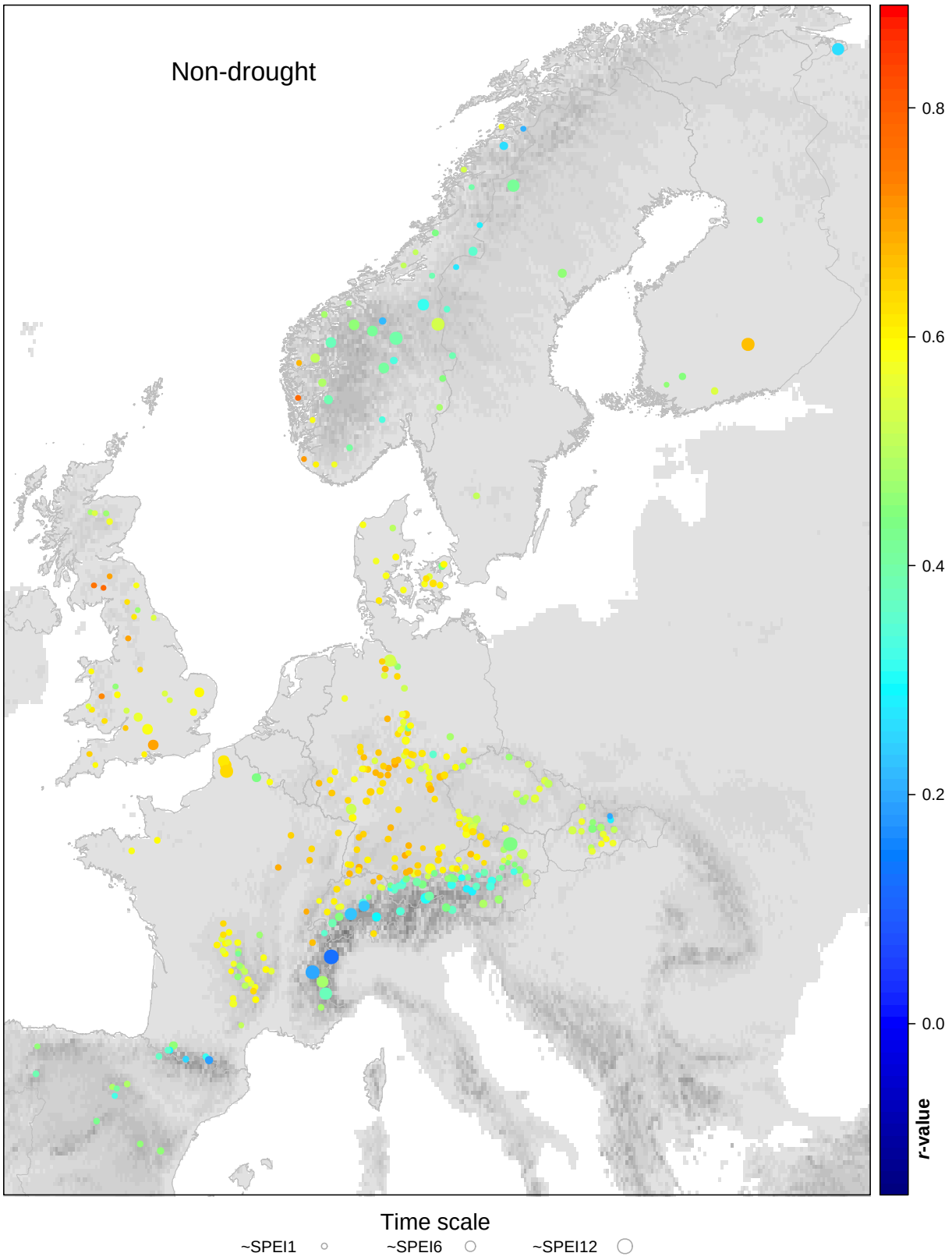

Figure 4.4: Maximum strength of the correlation between both indicators and the respective SPEI time scales (1-12 months) during non-drought conditions.

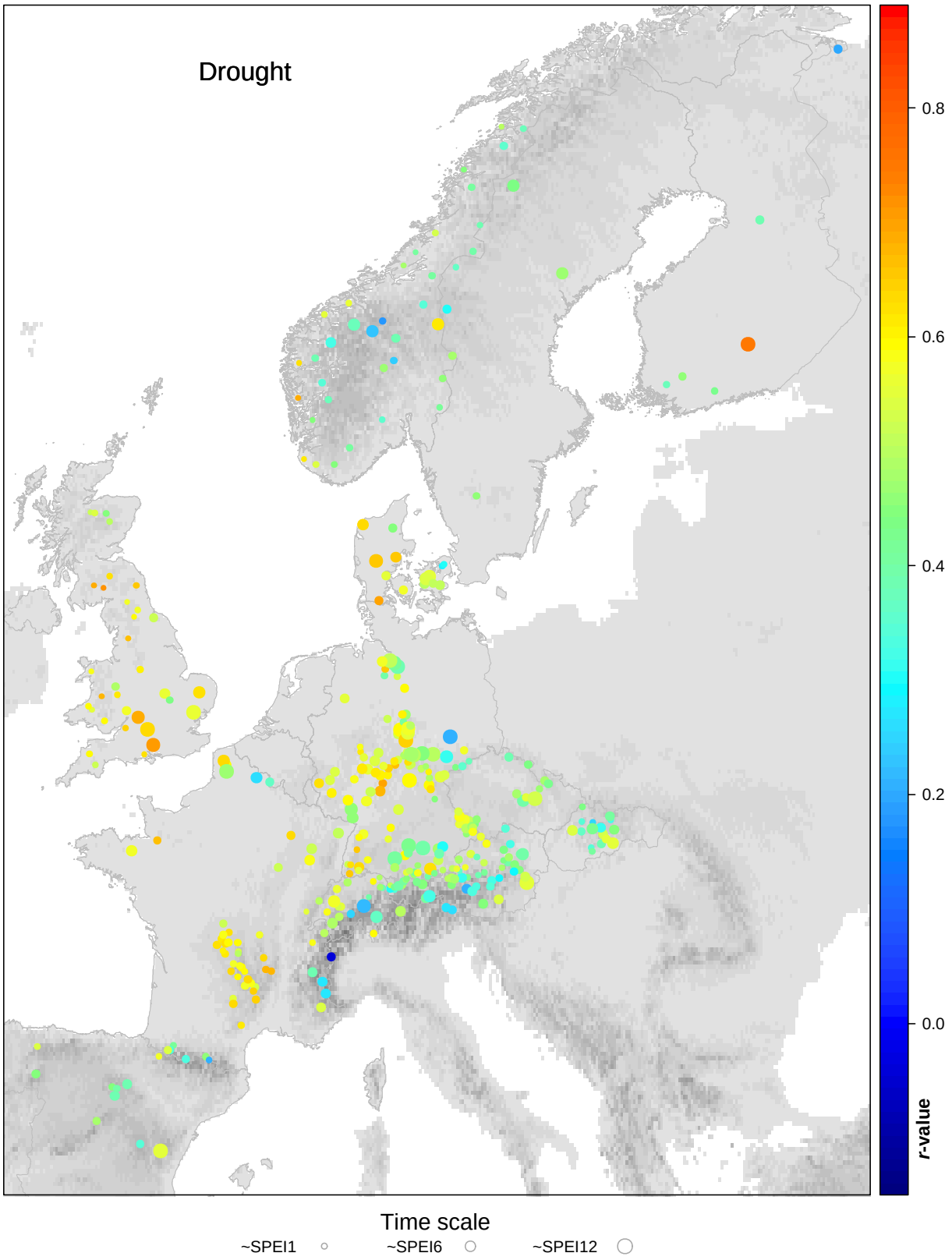

Figure 4.5: Maximum strength of the correlation between both indicators and the respective SPEI time scales (1-12 months) during periods of streamflow drought.

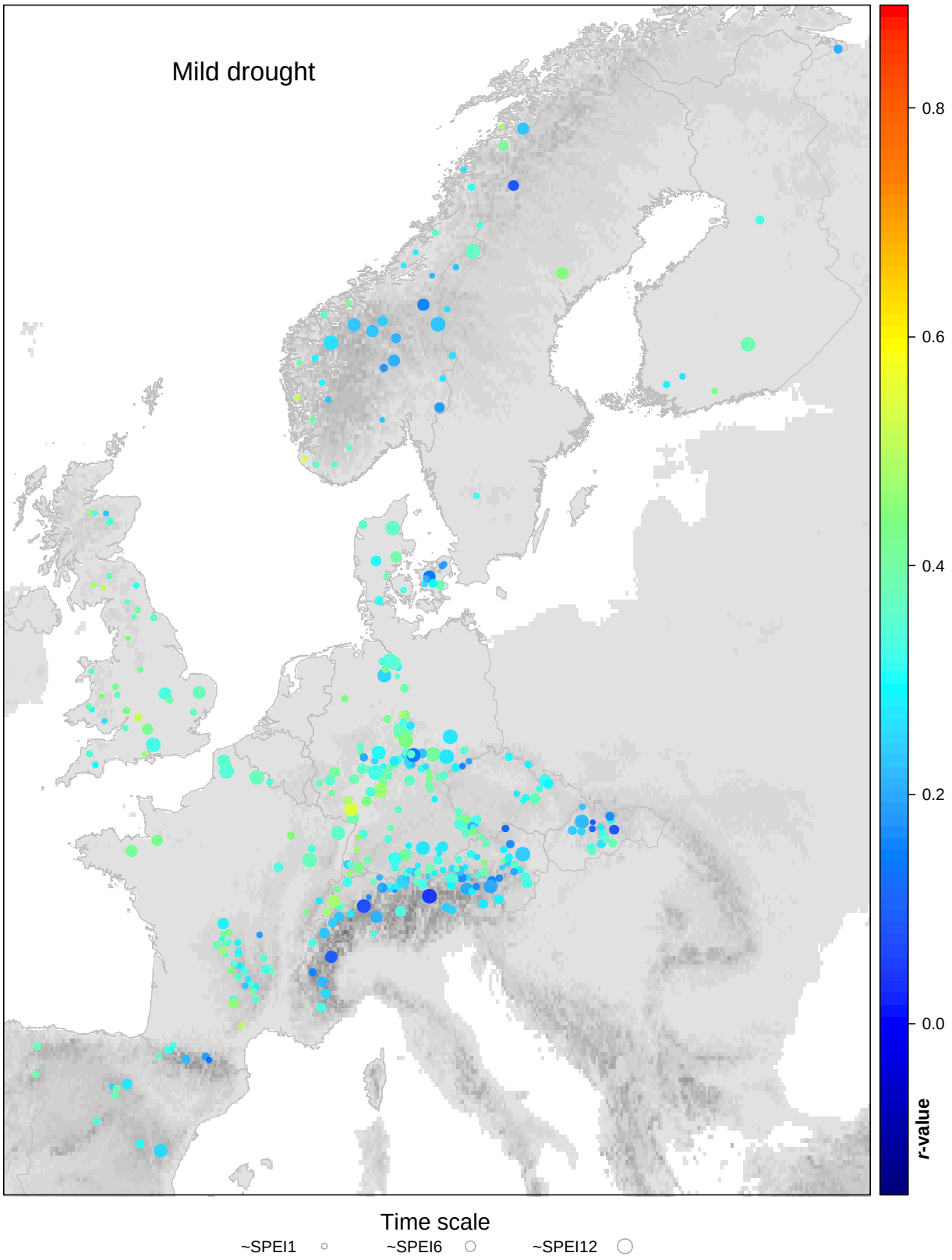

Figure 4.6: Maximum strength of the correlation between both indicators and the respective SPEI time scales (1-12 months) during periods of mild streamflow drought.

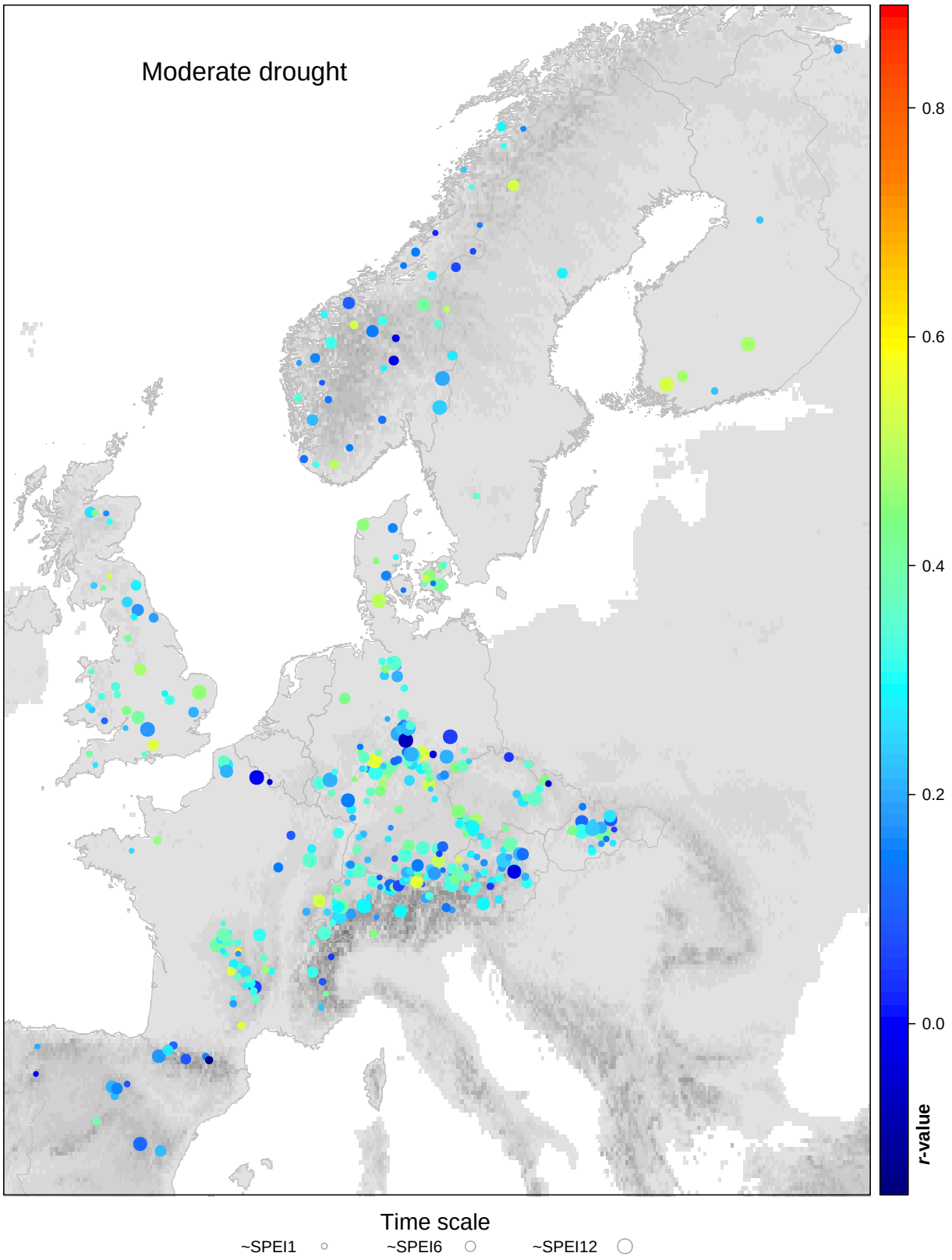

Figure 4.7: Maximum strength of the correlation between both indicators and the respective SPEI time scales (1-12 months) during periods of moderate streamflow drought.

Table 4.1: Percentage of peak *r*-values per SPEI time scale in relation to streamflow conditions.

Drought state	SPEI time scale											
	1	2	3	4	5	6	7	8	9	10	11	12
Complete series	10.2	40.7	16.0	16.5	4.7	4.7	1.0	1.3	0.3	1.3	0.8	1.6
Non drought	21.5	52.0	9.2	7.6	2.1	0.5	2.6	1.0	1.3	1.0	0.5	0.3
Drought	6.0	19.9	14.4	21.0	8.7	10.5	5.5	1.8	3.4	1.0	1.0	4.2
Mild drought	11.0	23.6	17.3	12.1	8.4	7.3	3.7	1.6	3.7	1.3	2.9	3.4
Moderate drought	14.7	15.2	11.0	11.0	7.1	4.2	5.0	3.7	3.7	5.2	3.7	6.3
∑	13.1	31.3	14.1	14.1	6.4	5.6	3.7	2.0	2.6	2.1	1.8	3.3

In conclusion, most catchments show their strongest correlation to varying climatic conditions, when these are integrated over short time scales (1-4 months) with a maximum response in case of the 2-month SPEI. Even though the connections between the SSI and SPEI at long time scales become weak, the slight increase of maximum *r*-values at SPEI scales of 12 months during streamflow droughts indicates that there are several catchments with long hydrological memory. Figures 3.3 to 3.7 show the highest coefficients of correlation between both indicators and the respectively associated time scales of the SPEI. The strongest correlations for the respective time scales are herein again visualized for the whole period of investigation as well as a function of each hydrological state. Figure 3.3 indicates a high degree of linear connections between the standardized series for most of the incorporated catchments across Europe. Correlation coefficients are mostly medium to high in magnitude in case of the complete time series and strongest relations are predominately found for small time scales.

In a spatial context, topmost *r*-values obtained for catchments along the main ridge of the Scandinavian Mountains, the Alps and the Pyrenees are relatively weak. For the first two mountain ranges, the occurrence of topmost correlations transpires towards values of the SPEI at intermediate and long time scales. Regions with highest correlations are in Denmark, Germany, France and the UK. Several catchments situated in the fjords of Western Norway also exhibit remarkably high maximum *r*-values.

When separating the whole period of investigation into hydrological drought and non-drought events, three major features can be emphasized, as visualized in Figure 3.4 and Figure 3.5. For both threshold levels, a distinct decline of maximum *r*-values for the majority of catchments appears compared to the overall time series. As the respective SPEI time scales of the peak correlation coefficients seem to be more or less stable for time steps with relatively high discharge corresponding *r*-values during hydrological

drought tend to shift towards longer temporal aggregations. In cases of both threshold ranges, the regional distribution of catchments with relatively low peak correlation coefficients remains the same on the whole. In the spatial context, patterns highlight lower peak *r*-values for the Alpine Region, Scandinavia, Spain, as well as Eastern Austria and most catchments in Slovakia and the Czech Republic. For mild and moderate states of hydrological drought, Figure 3.6 and Figure 3.7 reveal a further drop of topmost correlation coefficients for the entire dataset. In case of the former state, mainly weak correlations are obtained with almost the same regional distribution of extremely low *r*-values as for hydrological drought and non-drought events. Nonetheless, the absolute range of peak correlations decreases in the time of this condition. For moderate drought, maximal *r*-values and corresponding SPEI time scales lack a clear spatial pattern.

4.3 Clusters of the continuous linkage between both indicators

5 homogeneous clusters were obtained by hierarchical clustering of all scale-dependent correlation series. The clusters summarize the different curves of *r*-values and give a general picture of the reaction of all incorporated catchments to meteorological water balances as a function of time. Figure 3.8 shows the progression of the 5th, 25th, 50th and 95th percentiles of clustered correlation coefficients between the continuous series of the SSI and the individual SPEI time scales. Boxplots in Figure 3.9 summarize mean values of elevation, slope, precipitation, temperature and area for each cluster.

Cluster C_C1 consists of 50 catchments and is characterized by comparatively low catchment responses at shorter SPEI time scales and a strong increase of correlations to a time scale of 6 months. For further expanding scales, the percentiles indicate that correlations remain on a generally high level. As shown in Figure 3.10, the spatial distribution of catchments included in cluster C_C1 does not illustrate any significant regional patterns. Cluster C_C1 categorizes river networks of generally larger areas with minimum values of mean elevation, slope and precipitation when compared to the other clusters. Though cluster C_C1 exhibits the highest median of mean temperature values among all classifications, remaining quartiles for this cluster illustrate a large range of this climatic feature, especially towards lower temperatures.

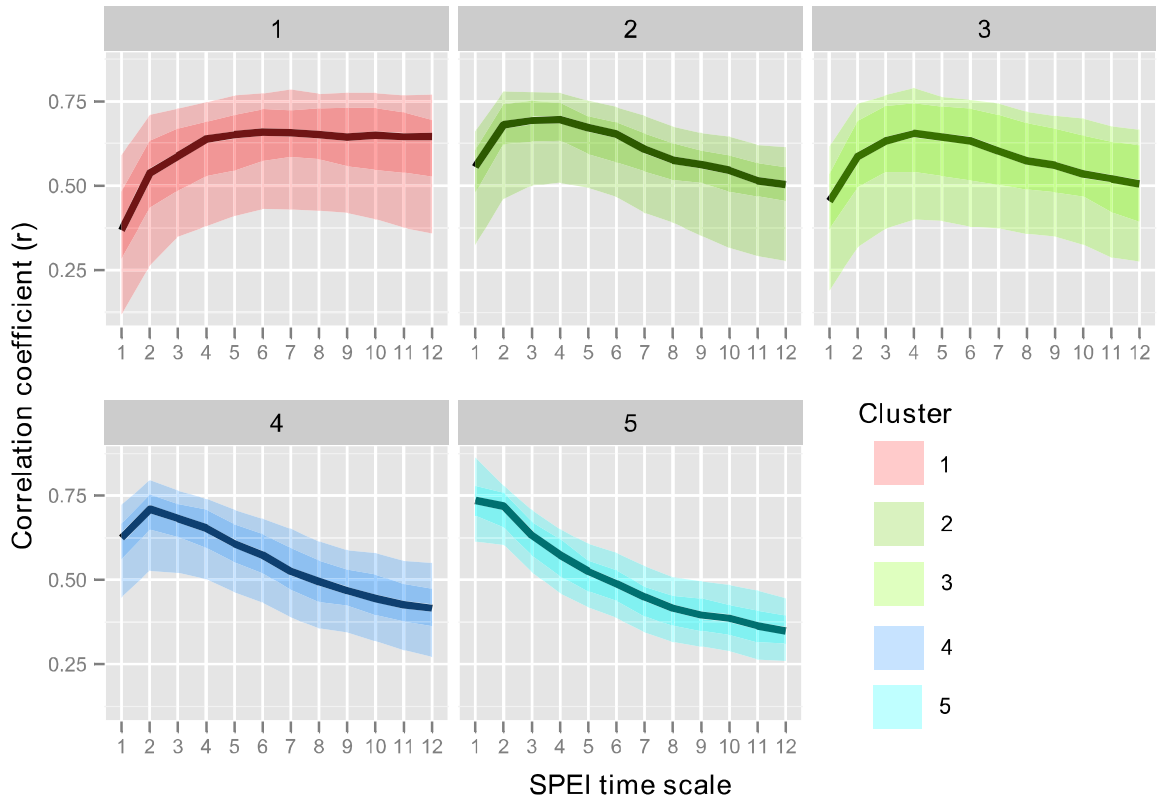

Figure 4.8: Progressions of obtained *r*-values over varying time scales of the SPEI for each cluster (C_C) of the continuous correlation. The 5th, 25th, 50th and 95th percentiles are indicated by transparency.

The 83 and 55 catchments classified in cluster C_C2 and C_C3 show their maximum response at a time scale of 4 months, referencing the progression of their 50th percentiles. Additionally, they are characterized by a relatively smooth and more evenly spread progression of correlations, as most their medians of scale-dependent *r*-values are almost exclusively above 0.5. Both clusters differ in terms of their variance. The 5th and 95th percentiles of cluster C_C2 indicate a moderate degree of homogeneity, whereas cluster C_C3 features a larger span of correlation coefficients. As for cluster C_C1, the geographical allocation of all catchments grouped in clusters C_C2 and C_C3 do not allow further interpretations of regional patterns. The similar reaction of streamflow to varying meteorological scales of both clusters is also expressed in terms of their uniform environmental properties. In comparison, classified catchments are moderately large, step and located at intermediate elevations. Both exhibit relatively low amounts of precipitation and the 25th and 50th percentiles of mean temperature values are lowest in case of cluster C_C3.

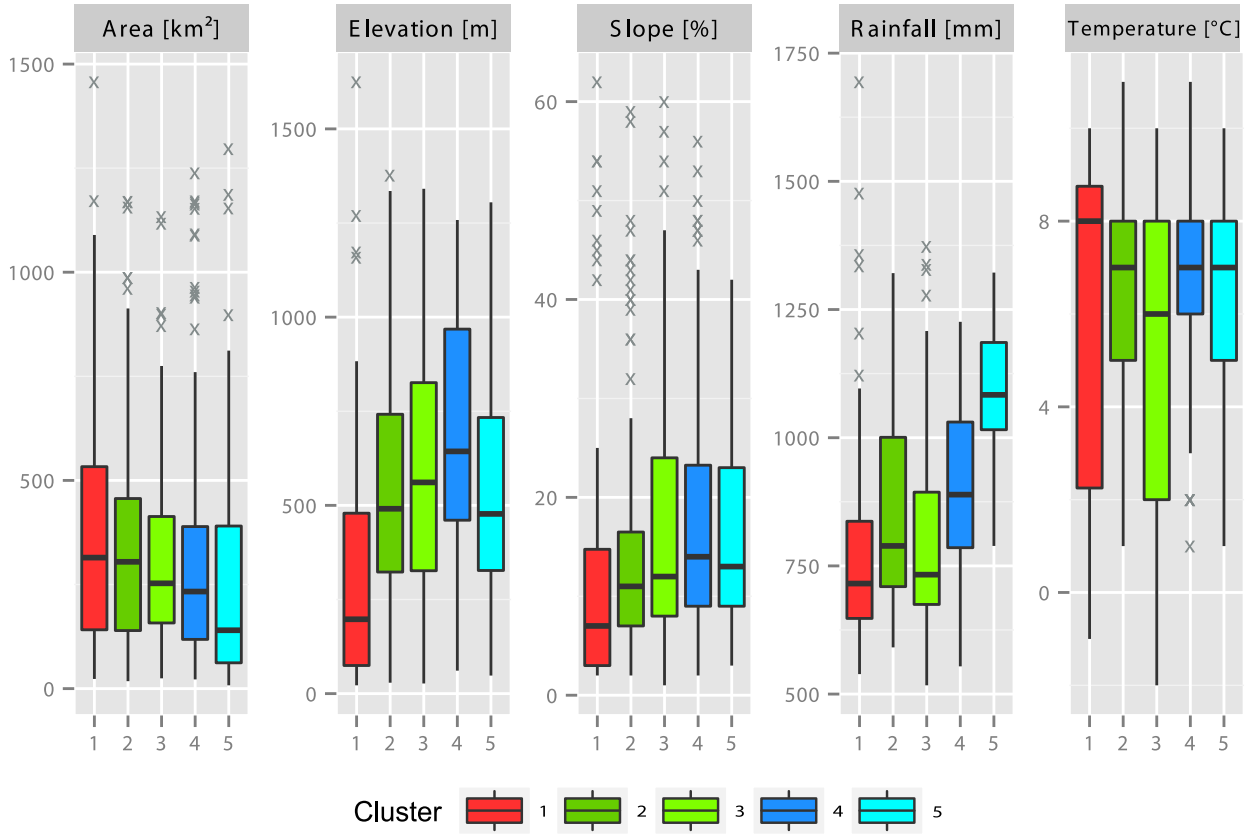

Figure 4.9: Box plots for mean values of surface area, elevation, slope, rainfall and temperature for those catchments represented by each cluster (C_C) of the continuous correlation analysis.

Fast responding catchments are summarized in clusters C_C4 and C_C5, which are identified by highest correlations for SPI time scales of 1 and 2 months respectively. Both curves show a continuous decrease of linkage with increasing time scales. With 132 classified catchments, cluster C_C4 represents the largest number of analyzed rivers. Cluster C_C5 stands out due to the minimum overall variance of *r*-values, expressed by the curves of its the 5th and 95th percentiles. In case of cluster C_C5, the 50th percentile of *r*-values calculated for a SPEI of 12 months exhibits the overall minimal strength of the link among all clusters, whereas the interrelationships are highest for the shortest available SPEI scale. The characteristic *r*-value curves of cluster C_C5 also mark an exception in relation to their regional allocation. Associated basins are spatially concentrated along the northern foothills of the Alps, in western and northern parts of the United Kingdom and in Western Norway. Catchments represented by clusters C_C4 and C_C5 have the smallest surface areas but exhibit generally higher values of mean elevation, slope and rainfall amounts. Cluster C_C4 categorizes basins with the highest mean altitudes and cluster C_C5 marks the maximum of mean precipitation of all clusters.

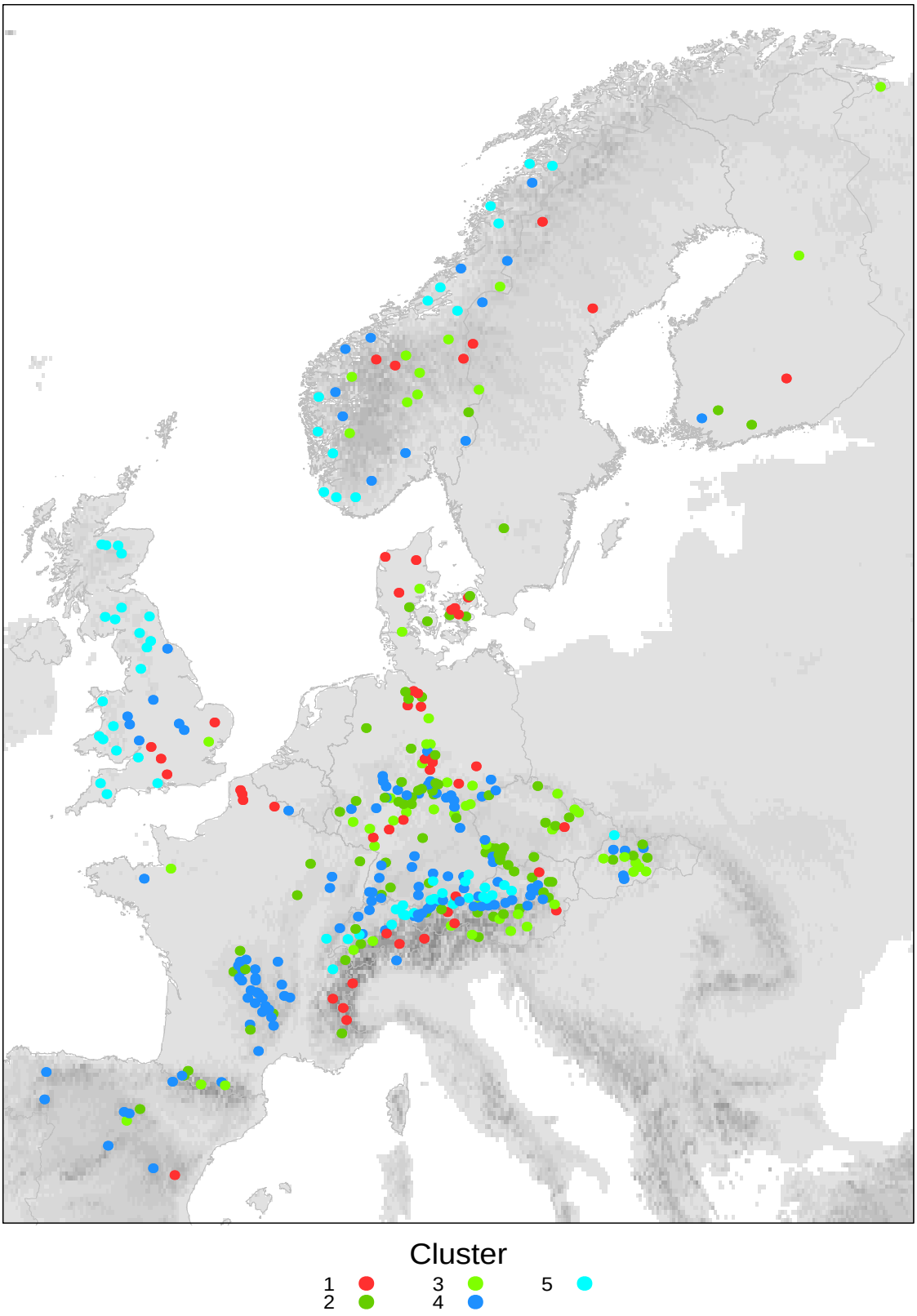

Figure 4.10: Spatial distribution of the clusters (C_C) of the continuous correlation analysis.

4.4 Hydrological regimes

The cluster analysis classified all catchments according to their seasonal runoff behavior, which is quantified by their monthly series of Pardé-Coefficients. The 10 resulting regimes summarize the high spatiotemporal variability of streamflow throughout the year and across Europe. Additionally, the classification mostly corresponds with previously set up categorizations of European rivers and their seasonal discharge variations (KRASOVSKAIA ET AL., 1994; ARNELL ET AL., 1993).

Several regimes (C_r1, C_r2, C_r3, C_r4, C_r5) are characterized by low flow periods during winter and discharge peaks during spring and summer months (Figure 3.11). As can be seen from Figure 3.12, these are mostly located at high altitudes of the Scandinavian Mountains (C_r2), further inland the Scandinavian Peninsula (C_r1), the western coast of Norway (C_r5) and the Alps (C_r2 and C_r4). Catchments clustered in regime C_r3 show similar seasonal runoff characteristics but are mainly located in two distinct regions: Southern Scandinavia on the one hand and along the mountain ranges of the Krkonoše (Czech Republic) and the High Tatra Mountains (Slovakia) on the other hand. The regional distribution of these regimes highlights the influence of storage and melting effects attributed to snow. During winter months precipitation is predominately stored as snow in higher altitudes and latitudes. Additionally northern Scandinavian rivers are frozen during winter (STAHL, 2001) and spring floods occur more rapidly due to snowmelt. This explains the strong decline of Pardé-coefficients in cases of regimes C_r1 and C_r2. Mountainous regions in the Alps (C_r4) are characterized by a more continuous progression of the high flow season, because catchments cover large ranges of altitudes. This circumstance affects the temporal behavior of snow accumulation and melting. Therefore peak flows during summer months and low flows during winter exhibit a more balanced character. Nevertheless, some catchments in alpine regions show a similar runoff behavior to mountainous regimes in Scandinavia (C_r2). These effects increase for runoff regime C_r3, because the influence of snow is herein reduced as a consequence of lower altitudes and latitudes of classified catchments.

Oceanic regimes (C_r6, C_r7, C_r8) ,predominantly following seasonal climate patterns, are located across Western Europe and northern parts of Central Europe with a winter maximum and a summer minimum. Catchments represented by regime C_r9 are mostly localized in low mountain ranges of Central Europe, the Czech Republic and Slovakia.

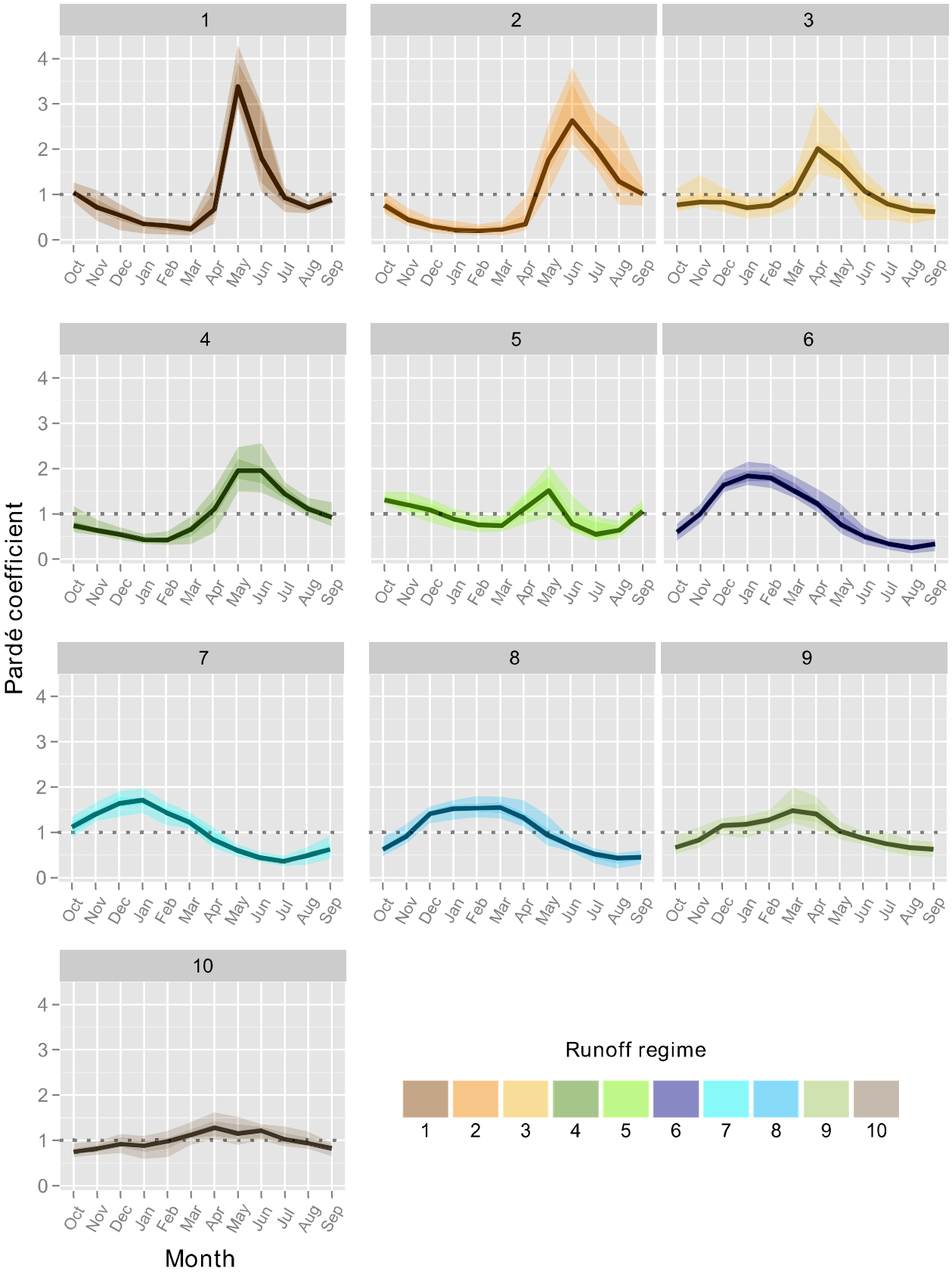

Figure 4.11: Runoff regimes (C_r) of the clustered catchments. The 5th, 25th, 50th and 95th percentiles of monthly Pardé-coefficients are indicated by transparency.

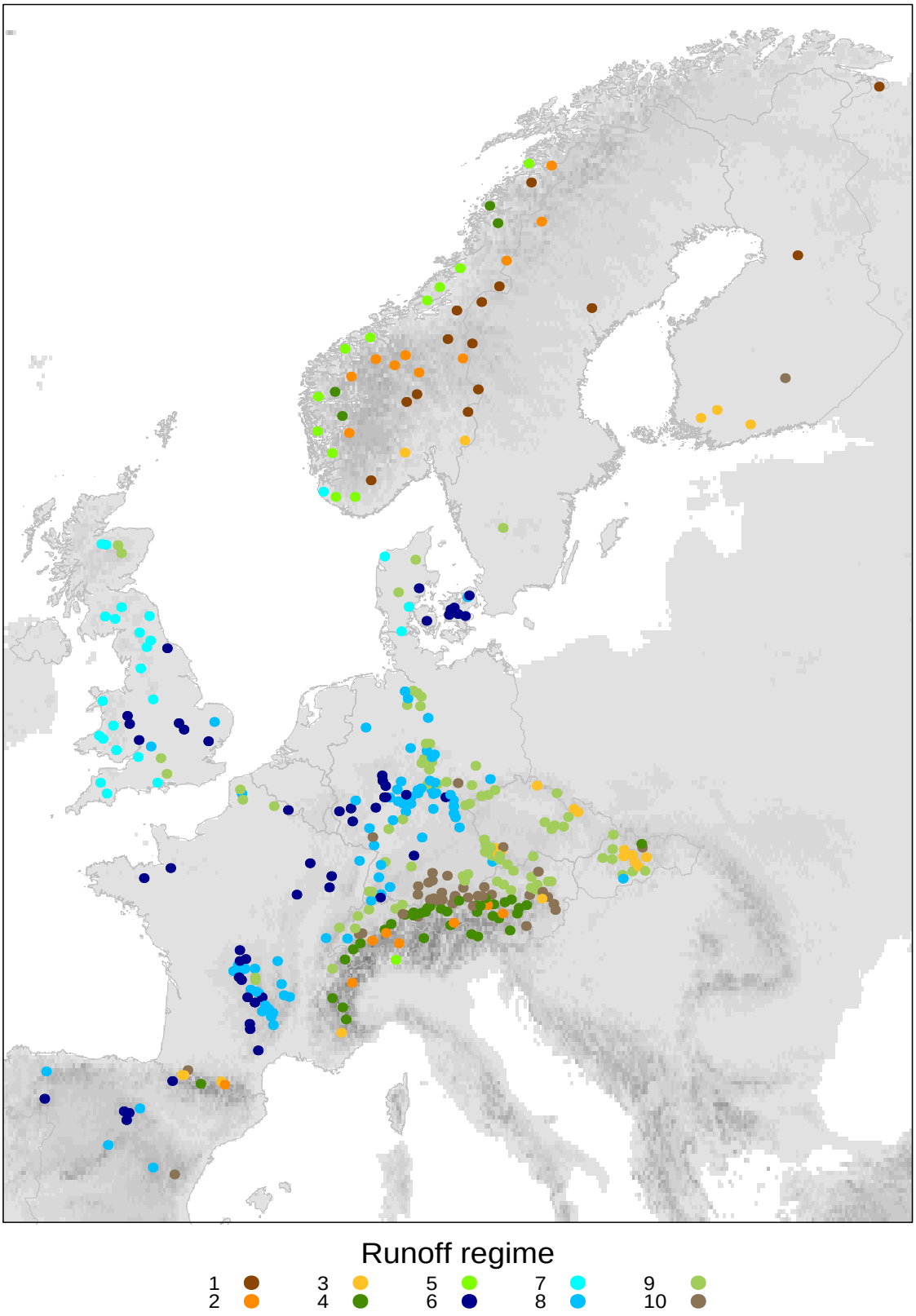

Figure 4.12: Location of the catchments represented by each runoff regime (C_r).

Runoff patterns exhibit an oceanic character with high flows during winter and spring and low flows during summer months, but are also influenced by nival conditions. These result in depressed peak flows during early winter and smoother seasonal variations.

The slightest streamflow fluctuations throughout the year can be observed for regime C_r10, which is geographically concentrated in the Alpine foothills of Austria, Germany and Switzerland. This classification exhibits a maximum in spring and early summer due to snowmelt and a minimum in autumn and winter. The balanced character of seasonal streamflow variations can be explained by the impacts of lakes and groundwater in this post glacial environment (BAUER ET AL., 2003).

Regime C_r5 is a complex regime type and classifies catchments, which are exclusively distributed along the Norwegian coastline. Superposition of snowmelt effects and oceanic climate patterns can be seen as driving force of seasonal runoff variability. Low flow seasons are during late winter and summer and an additional high flow season occurs from autumn rain.

It is noteworthy that most catchments in the Pyrenees are classified into different nival-glacial flow regime types. In conclusion, it can be stated that overlapping effects of all analyzed river networks can be ignored due to their relatively small areas. This assumption is confirmed by the fact that all series of monthly Pardé-coefficients exhibit only one maximum of normalized streamflow per year, except for regimes C_r3, C_r5 and C_r10.

Regimes C_r1 and C_r2 have the lowest overall linkage between the SSI and the SPEI, which is elucidated by the relatively weak correlations among all time scales (Figure 3.13). In case of the former regime (C_r1), there is a sharp increase of correlations from shortest towards intermediate time scales of the SPEI (4-6 months), which mark a balanced peak before the level of interrelation decreases with further increasing scales. The same course of correlation coefficients can be observed for regime C_r2**,** but with a comparably low level of connection and maximum *r*-values at SPEI time scales of 4-6 months. Interquartile ranges of *r*-values express the topmost variability of correlations between the SPEI and the SSI among all hydrological regimes. Conversely, regime C_r1 is characterized by rather low ranges of *r*-values except the case of the monthly SPEI.

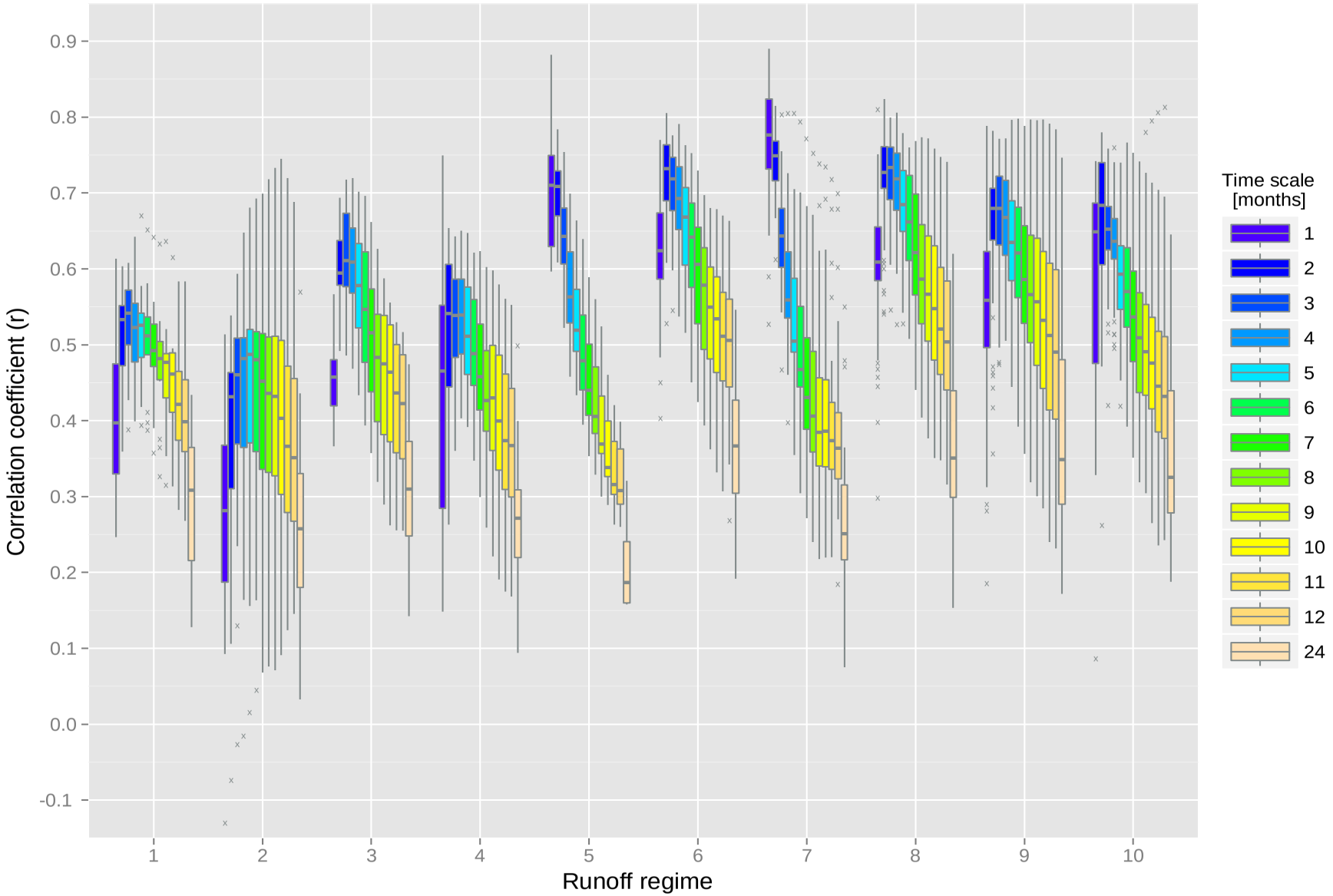

Figure 4.13: Box plots of correlations between continuous series of the SSI and the SPEI at different time scales for each runoff regime (C_r)

Intermediate levels of general correlation can be seen in the case of regime C_r3 with an exceptionally sharp increase of correlation from SPEI time scales of 1 month towards 2-4 months. Additionally, interquartile ranges of correlations appear to increase with greater scaling.

The interquartile range of *r*-values for the monthly SPEI in case of regime C_r4 marks the highest level of variation among all other temporal aggregations. Levels of correlations reach their maximum at SPEI scales between 2 and 4 months and continue to decline thereafter.

Degree of correlation in case of regime C_r5 is highly dependent on the chosen temporal aggregation of the SPEI. Peaking at SPEI scales of 1 and 2 months, quartiles of *r*-values show a steep downward trend approaching larger scales. While correlation coefficients for the shortest scales rank among the highest compared with other regimes, the longest SPEI scales exhibit the lowest levels of relationship between climatic variability and runoff behavior.

Hydrological regimes C_r6, C_r8 and C_r9 exhibit similar progressions of quartiles. Peak correlations at SPEI time scales of 2 and 3 months follow close upon minimal correlations at monthly scales. The connection declines with higher levels of the SPEI. A remarkable feature of regime C_r9 is that its 50^{th} quartile at a time scale of 1 month ranks lowest but its interquartile range covers the widest spectrum of *r*-values among the three related clusters.

Like regime C_r5, regime C_r7 is characterized by an exceptionally high dependency of correlation on the respective SPEI time scale. Another peculiarity of this regime is its superior degree of correlation at time scales of 1 and 2 months when compared to the remaining clusters of seasonal runoff variations. Between scales of 2 and 3 months correlations record a significant decline, which continues with further increasing temporal aggregations.

Quartiles of *r*-values in case of regime C_r10 are mostly coinciding with those of regimes C_r6, C_r8 and C_r9. Nevertheless, the interquartile ranges at SPEI time scales of 1 and 2 months are comparably high and the median of correlations at the monthly SPEI indicates a stronger relationship between short-term climatic water balances and streamflow patterns.

4.5 Monthly correlation patterns between the SPEI and the SSI

The 15 cluster solution yielded consistent results in terms of intra-cluster homogeneity and regional allocation. Figure 3.14 shows the mean correlations between the monthly series of the SSI and the SPEI for each of the 15 groups, obtained by the hierarchical cluster analysis. There are remarkably differences between the monthly relationships of the 15 clusters in terms of their seasonality and overall linkage. Intra-cluster heterogeneities of derived correlation coefficients are shown in Figure 3.15. Spatial distribution and main environmental characteristics of all clusters are visualized in Figure 3.16 and Figure 3.17.

The 14 Catchments of cluster C_m1 are widely distributed across continental Europe. River basins of this classification can be found in Austria, Slovakia, the French Alps and Northern Denmark but there is also a noticeably geographical concentration in the North German plain. Regarding their main physiographical properties, catchments of this cluster are moderately large, located on low altitudes and exhibit the lowest values of steepness and precipitation when compared to the other clusters of seasonal linkages. Values of mean temperature are generally high. Cluster C_m1 is characterized by relatively high correlations throughout the year when compared to other classifications. Patterns of *r*-values highlight the independence of streamflow response from the chosen time scale of the SPEI. However, seasonal discrepancies can be observed with rather low correlations in February for all temporal aggregations of the meteorological drought index and comparably high mean *r*-values in spring (at SPEI time scales of 2-4 months), late summer and autumn (at SPEI time scales of 2-12 months). A remarkably feature of cluster C_m1 is the high level of overall variations regarding the seasonal correlations of its clustered catchments. Intra-cluster variations of monthly *r*-values reach their maximum during winter (at all time scales of the SPEI) and in April and June (at shorter SPEI scales). The highest heterogeneity among all computed clusters is also highlighted by the high geographical dispersion of all involved catchments.

Cluster C_m2 consists of 16 catchments, which are exclusively located in the mountain ranges of the Alps. Its mean values of elevation, slope and precipitation are ranked highest among all obtained clusters, whereas mean temperatures are considerably low. Connections between seasonal climate variability and streamflow of cluster C_m2 can be summarized as generally low.

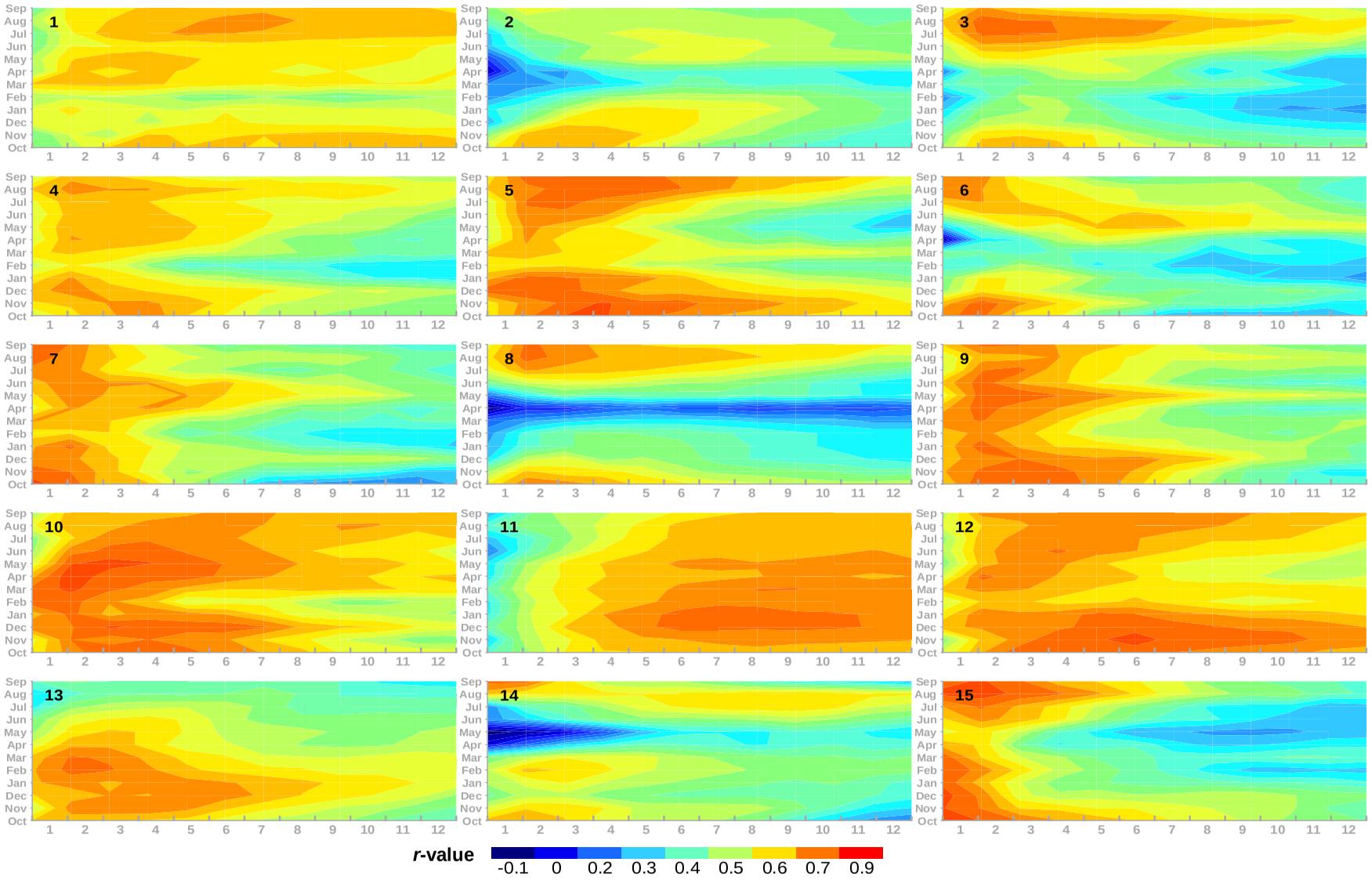

Figure 4.14: Correlation patterns of the monthly SSI and SPEI series according to the hydrological year (y-axis). The x-axis represents the different SPEI time scales. The contour plots show the average *r*-values of each derived cluster C_m.

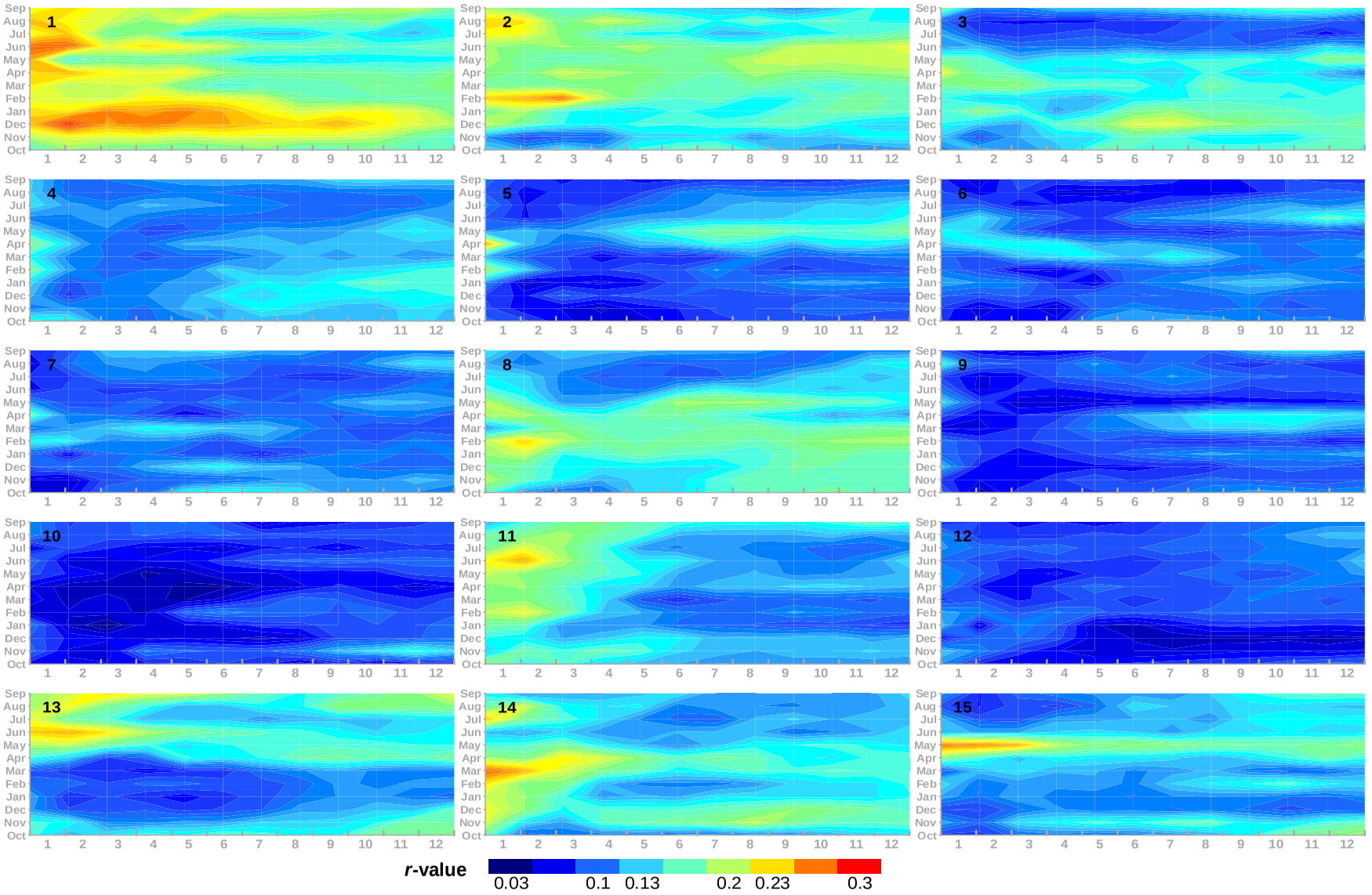

Figure 4.15: Standard deviation of monthly correlations within each cluster C_m.

Weakest correlations occur during the February-May period especially in case of short SPEI scales but stay on a generally low level when aggregations of the SPEI increase. From October to January, high correlations can be found at SPEI time scales of 1-7 months. In summer, correlations mark a second seasonal peak and are related to intermediate SPEI time scales (5-8 months). As in case of cluster 1, this classification (C_m2) exhibits a high standard deviation of *r*-values in February (at SPEI time scales of 1-3 months) as well as in July and August (at SPEI time scales of 1-2 months).

22 river basins are classified in cluster C_m3. They are situated in three distinct regions: the Eastern Central Alps in Austria, the High Tatra Mountains in Slovakia and the mountain ranges of the Sudetes in the Czech Republic. The mountainous character of these catchments is elucidated by their relatively high elevation and steepness, as well as their comparably low values of mean temperature throughout the year. Cluster C_m3 is characterized by weak correlations during winter and early spring on the one hand and high *r*-values during summer and autumn. These are mostly not influenced by respective time scales of the SPEI. The investigated relationship exhibits a maximum level in August, if SPEI time scales of 2-3 months are considered. During the period of maximum linkage, cluster C_m3 exhibits a low level of standard variation in terms of its seasonal variations. This can be seen as an indicator for the overall similarity of peak hydrological responses of all included catchments.

Rivers associated with cluster C_m4 are mainly located in the northern Alpine foothills of Austria and Germany, in the Bavarian Forest and also in central parts of the Czech Republic and the Slovak Ore Mountains. Additionally, some catchments are situated on the southern edge of the Massif Central and in the Pyrenees. The 44 basins of cluster C_m4 are located in rather high altitudes and exhibit a wide range of steepness. Values of mean annual precipitation and temperature are in a moderate range when compared with the remaining clusters. From October to January, relation coefficients are on a high level in case of cluster C_m4. A drop of correlations can be observed during February, especially for longer time scales of the SPEI. Another maximum of interrelation can be found from spring until September with monthly increasing explanatory power of higher SPEI scales. Standard deviation of correlations between the monthly series is generally small at all SPEI time scales.

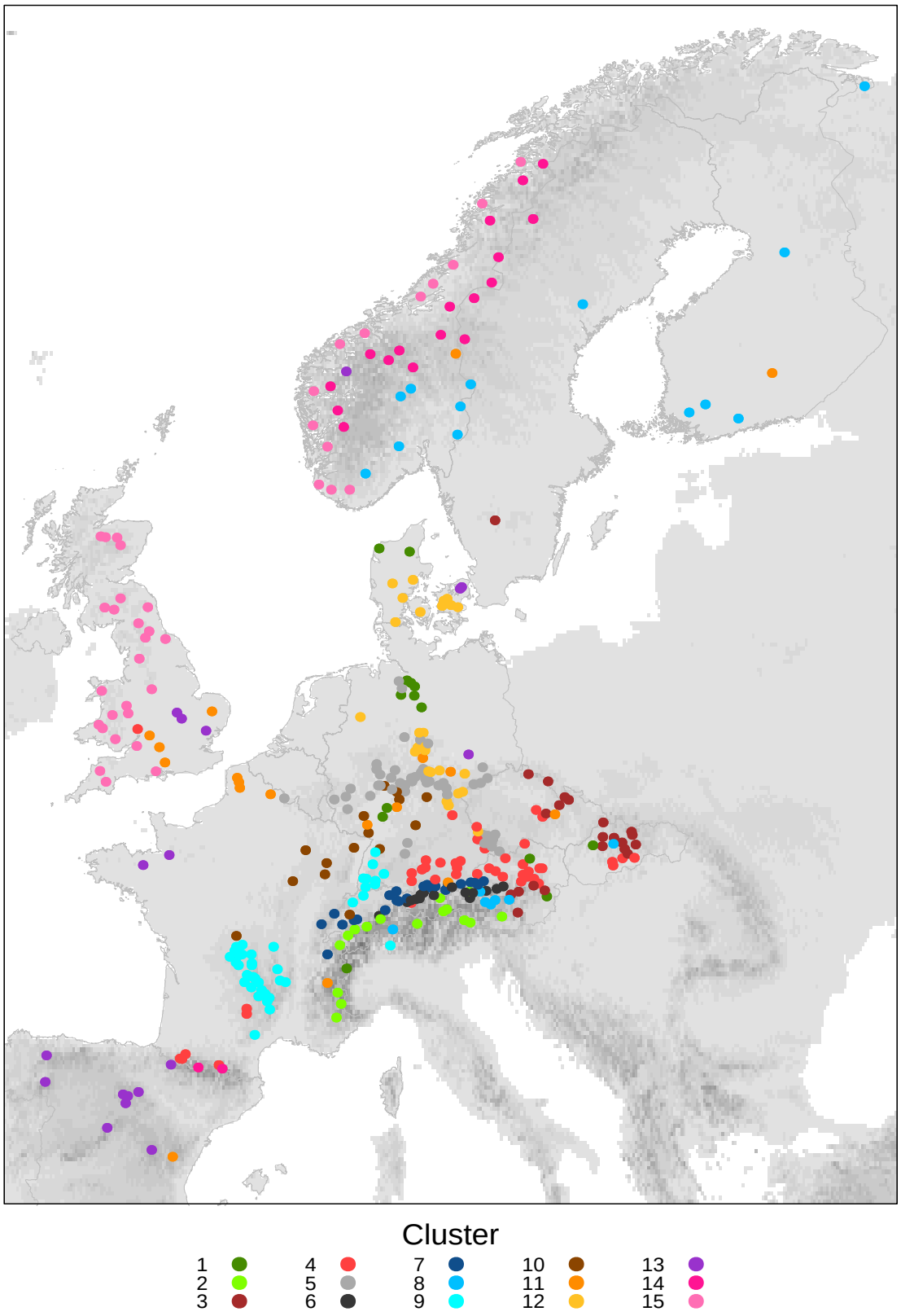

Figure 4.16: Location of the catchments represented by each cluster of the monthly correlation (C_m).

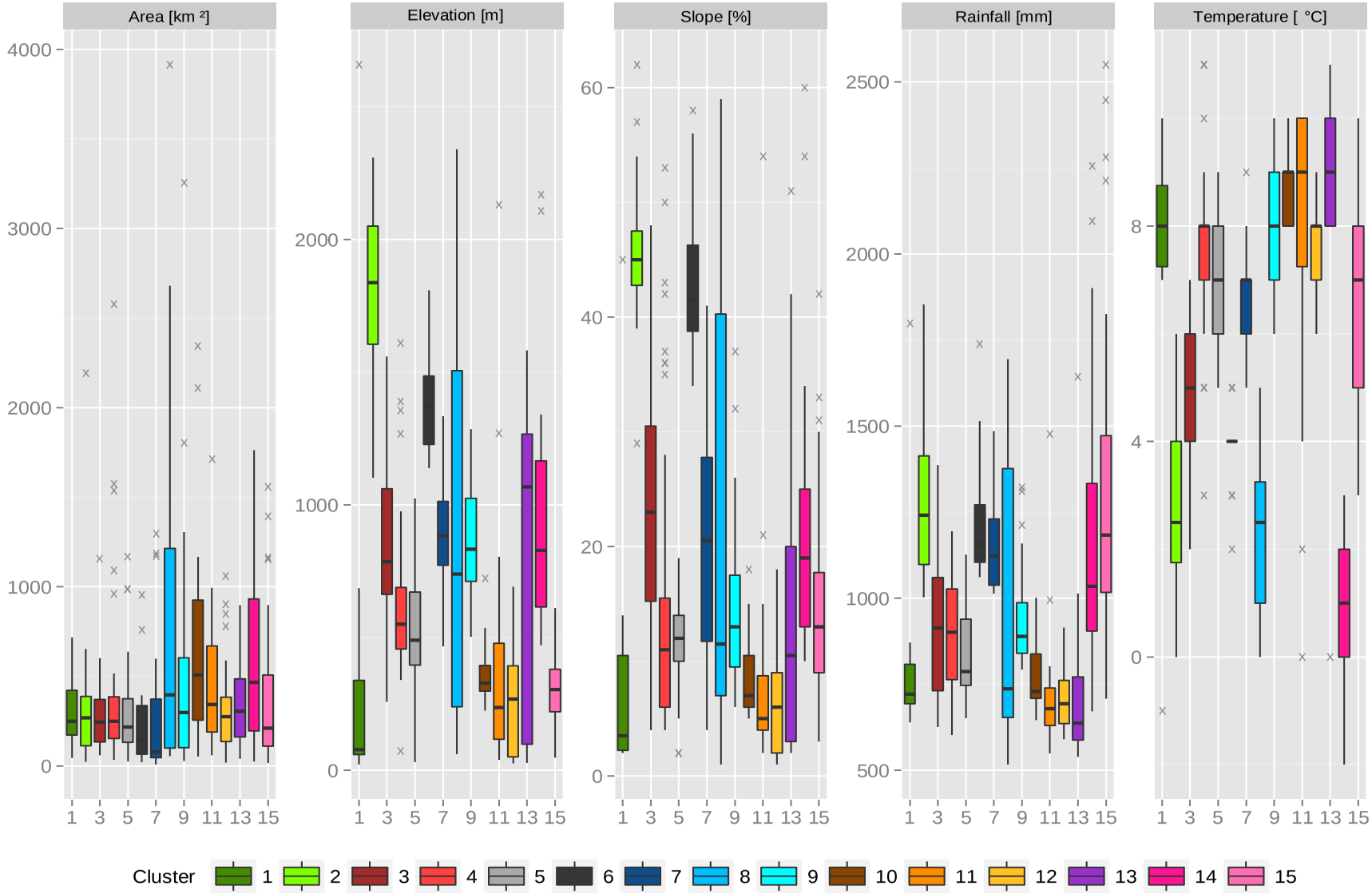

Figure 4.17: Box plots for mean values of surface area, elevation, slope, rainfall and temperature for those catchments represented by each cluster (C_m) of the monthly correlation analysis.

Cluster C_m5 summarizes 55 catchments, which are predominately situated in the Central German Uplands and the Bavarian Forest. Typical environmental characteristics of these low mountain ranges are reflected in the remarkably similarity of cluster C_m5 to cluster C_m4. Both classifications exhibit largely identical properties and typical seasonality of correlations. Mean *r*-values of Cluster C_m5 are generally high in comparison with other classifications. The cluster is furthermore characterized by strong correlations for all SPEI time scales during late summer, autumn and early winter. A maximum of correlation is observed from August to October in case of SPEI time scales of 2-5 months. In spring, the interrelation tends to be rather low, especially for higher temporal aggregations of the SPEI. Even though standard deviations of *r*-values are relatively small, the obtained correlation coefficients between the SSI and the monthly SPEI exhibit a strong degree of heterogeneity in April.

16 streams are summarized in Cluster C_m6. They are exclusively located in valleys along the northern mountain ranges of the Alps in Austria, Germany and Switzerland. It is noticeable that all catchments are situated on an imaginary line between East and West and at only slightly differing altitudes. Therefore catchments of cluster C_m6 are on higher elevations and exhibit very steep slopes, high amounts of precipitation and low annual mean temperatures. Peak correlations of cluster C_m6 can be found during autumn when the monthly SSI is compared to SPEI time scales of 1-4 months and during summer when compared to longer time scales. Weakest correlations are obtained during late winter and early spring with a distinct decline of linkage in April at a SPEI time scale of 1 month. Cluster C_m6 is furthermore characterized by low standard deviations throughout the year and among time scales of the SPEI when compared to other clusters. Higher variations of correlation coefficients can be obtained in spring at time all scales of the SPEI.

Catchments represented by cluster C_m7 exhibit a geographical concentration on the border between the Northern Alps and the prealpine lands as well as in the central regions of the Swiss Jura. The 24 associated river basins register high values of mean elevation and precipitation. Mean annual temperatures indicate a relatively cold alpine climate. Cluster C_m7 is furthermore characterized by moderately high values of mean slope, but the interquartile range of this property illustrates a large variety of steepness among all river basins. The spatial distribution of cluster 7 is almost identical to cluster C_m6, but catchments of the latter cluster exhibit a more mountainous nature.

Monthly correlations obtained for cluster C_m7 are contrastive regarding the respective SPEI periods. Generally, SPEI scales from 1-4 months show high correlations with the SSI all over the year. Longer time scales lack a significant correlation with monthly streamflow. Exceptions are the *r*-values from April to June considering SPEI time scales of 1-5 months. In case of cluster C_m7, standard deviation of *r*-values can be summarized as relatively low in comparison with other classifications.

Cluster C_m8 consists of 20 basins, which are largely located in two distinct regions: While a group of catchments is situated in the Alps, some rivers are located on the Scandinavian Peninsula. One catchment is located in the High Tatra Mountains in Slovakia. Furthermore a separation can be made according to the respective natural environments of the Scandinavian catchments. While some rivers are located at the foothills of the southern Scandinavian mountains, several basins can be found further inland. The spatial heterogeneity is also reflected in terms of the cluster's physiographical characteristics. Interquartile ranges of nearly all incorporated properties rank highest among all obtained clusters. This impedes an unambiguous description of environmental influences on the linkage between the SSI and the SPEI. Generally low values of annual mean temperature constitute an exception for this cluster. Cluster C_m8 shows one of the highest dependencies of correlation to seasonal conditions. Nearly all SPEI time scales correlate well with standardized discharge series during autumn, but on a generally low level during the rest of the year with an absolute minimum in April. Peak correlations are obtained in August and September at a SPEI time scale of 2 months. This pattern visualizes the great overall variability of correlations when comparing streamflow anomalies to the meteorological drought index. The strong seasonality is furthermore highlighted by a strong degree of standard deviation during the December-June period at all SPEI time scales. A lower level of variation can be found throughout late summer and autumn. Largest variations are obtained in February when SPEI time scales of 1-2 months are considered and in June at SPEI time scales of 1-2 months.

Cluster C_m9 represents 39 catchments, which are predominately located around the Black Forest in Germany, in the northern parts of the Swiss Jura and all over the Massif Central in France. One river basin assigned to this cluster can also be found in Ticino, Switzerland. Moderately high elevations, intermediate values of slope and precipitation, as well as comparably high temperatures are the characteristics of this clus-

ter. Cluster C_m9 exhibits two seasonal maxima of correlation during the periods between October and December as well as between April and June at SPEI time scales of 3-4 months. During autumn and spring the cluster has its highest hydrological memory in terms of strong correlations at higher SPEI time scales. Patterns of correlation indicate a relatively high dependency of interrelation on the chosen SPEI time scale. In general, cluster C_m9 is characterized by a low level of standard deviation. Large intra-cluster variabilities can be found in March and April at longer SPEI time scales (7-12 months).

The majority of the 15 river basins represented by cluster C_m10 are spatially distributed across northwestern regions of France and western parts of Central Germany. The cluster is characterized by low values of elevation, slope and precipitation. In comparison to other clusters, this classification is defined by overall high values of temperature throughout the year. Cluster C_m10 is characterized by peak correlations from October to December and from March to Mai at SPEI time scales of 2-6. In general, the relationship is persistent and strong throughout the year and for most SPEI time scales. Lowest interrelations between the SSI and the SPEI are obtained for long temporal aggregations during November and January as well as during June and July when considering the shortest time scale. Cluster C_m10 exhibits very low standard deviations among all monthly correlation series.

The 18 catchments of cluster C_m11 exhibit a wide spatial distribution and lack of regional homogeneity. Geographical clusters can be observed in Southern England, Central Germany and Northern France. Cluster C_m11 is furthermore defined by lowland characteristics, as its typically small values of elevation and slope indicate. Additionally, catchments associated with cluster C_m11 are characterized by low amounts of annual rainfall and a rather warmer climate. Cluster C_m11 is defined by patterns of correlation which are mostly a function of the chosen SPEI time scale. Classified catchments tend to higher magnitudes of response with increasing temporal aggregations. Throughout the year, minimum correlations occur when the SSI is compared to the shortest SPEI scale and maximum *r*-values are found at SPEI time scales between 5 and 12 months. Herein, a slight seasonal dependency is obtained with peak correlations in December and January. There are large differences between the monthly correlation series of all clustered catchments, especially in February and June (at SPEI

time scales of 1-2 months). In general, the variation of *r*-values is higher when small SPEI time scales (1-6 months) are incorporated in the correlation analysis.

River networks of cluster C_m12 are concentrated around the Central German Uplands of the Thuringian Forest, the Harz Mountains and the Erzgebirge. Additionally, associated catchments can be found on the mainland part and on several isles of Denmark. Given these two distinctive regions, values of mean altitude and slope are rather low but with high intra-cluster variations. In comparison to other clusters, climatic conditions of the 28 included basins can be summarized as rather dry and warm. Seasonal streamflow and climate indicators are of generally high correlation at SPEI time scales from 2 months and upwards. This cluster is furthermore characterized by peak correlations from November to December at intermediate SPEI time scales. Cluster C_m12 exhibits a low level of standard deviation throughout the year and among all SPEI time scales.

18 catchments are associated with cluster C_m13, which has its geographical concentration on the northern half of the Iberian Peninsula. Additional catchments are situated near the coastlines of Brittany in France, in the East of England and on Zealand in Denmark. Regarding its environmental properties, cluster C_m13 is characterized by a high interquartile range of mean elevation and slope. All catchments have in common a marine west coast climate with a relatively low amount of precipitation and rather warmer temperature. Mean correlations obtained for cluster C_m13 are characterized by a high degree of seasonality. The classification exhibits high dependencies between monthly series of the SSI and the SPEI during autumn and winter and a poor relationship between the SSI and all time scales of the SPEI in summer. In the January-March period, absolute peak correlations are obtained at SPEI time scales of 2 months, but relatively high *r*-values are also computed for the remaining temporal aggregations (1-12 months). The standard deviation of correlation coefficients is strongly influenced by seasonality. During winter, *r*-values between the SSI and the SPEI are relatively homogenous, whereas in summer a large variation can be found among the clustered catchments, especially at shorter SPEI time scales.

Cluster C_m14 consists of 19 rivers, which are located in two different physical environments: the Central Pyrenees and the Scandinavian Mountains. Catchments represented by cluster 14 are generally situated at high mean altitudes and are rather steep. Additionally, they are characterized by moderate amounts of annual rainfall and

exceptionally low temperatures when compared to other classifications. Cluster C_m14 is characterized by strong correlations in autumn at SPEI time scales of 1-3 months and in winter at SPEI time scales of 2-4 months. In spring, the hydrological response to meteorological variations is very poor, especially at SPEI time scales of 1-4 months. During late summer, relatively high correlations are obtained when computed at longer scales of the drought indicator (5-12 months). Patterns of correlation indicate a strong seasonal influence on the response of streamflow to meteorological conditions. Standard deviation is comparatively high in case of cluster C_m14. Strongest deviations between the classified catchments are obtained from February to April (at SPEI time scales of 1-4 months) and in July and August (at SPEI time scales of 1-2 months).

Cluster C_m15 is geographically concentrated in the fjords along the coastline of Western Norway and in western and northern regions of the UK. Regarding their main physiographical properties, the 38 catchments of this cluster are relatively small and at low altitudes. Values of mean temperature and precipitation rank among the highest of all computed classifications. Correlations of cluster C_m15 are generally high over the hydrological year when shorter time scales of the SPEI (1-2 months) are considered. During late summer and autumn, correlations coefficients are also relatively strong with increasing SPEI time scales. High *r*-values during August, September and October mark the maximum of the hydrological memory for this cluster. Additionally, correlations remain strong with further temporal aggregations of the SPEI in February. During other seasons, larger scales of the SPEI lack a significant connection to streamflow variations. For these periods, correlations are among the lowest of all obtained clusters. In case of shorter time scales of the SPEI, standard deviation within cluster C_m15 is generally low. May is an exception with extraordinarily high variations among the correlation series, especially at a SPEI time scales of 1 month.

5 Discussion

5.1 Continuous relations between the SPEI and the SSI

The interrelation between the continuous series of the SSI and the SPEI at different time scales provides a general picture of streamflow reaction to meteorological drought indicators with varying time scales and under different conditions of surface water availability. In General, in can be stated that the explanatory power of climate indicators is highest, when the entire observation period is taken into account. Herein, most investigated catchments tend to rather short delayed response times to precipitation and evaporation conditions. When differing states of streamflow conditions are considered, the overall interrelations between the SPEI and the SSI are on the same level in case of drought and non-drought events. Nevertheless, the highest overall correlations during non-drought periods can be observed when meteorological conditions are integrated over an interval of 2 months. Contrary, the transfer time of water through the terrestrial part of the water cycle is way longer in cases of streamflow drought. A possible explanation for this shift of overall linkage towards higher time scales of meteorological signals could be the influence of preceding soil moisture conditions. When river discharge is relatively high, it can be assumed that basin storages are rather filled up and precipitation is sooner transformed to runoff. As opposed to this, streamflow drought can be seen as a function of depleted catchment storage. Regardless of total precipitation, rainfall during hydrological drought events primarily replenishes soil pores and aquifers. The almost complete lack of connection with further increasing levels of streamflow drought is an indication for the complexity of drought propagation. Transfers of water through the hydrological cycle result from natural processes, which cannot be seen in a temporally independent manner (VAN LANEN ET AL., 2012).

In the overall context it can be concluded that a SPEI of 2 months is most capable to assess the relative amount of river water resources. This outcome agrees with findings of previous investigations. Several regional case studies in Spain and Hungary demonstrated that streamflow generally shows the highest response when compared to meteorological drought indicators at time scales of 2 months (SZALAI ET AL., 2000; LORENZO-LACRUZ ET AL., 2010; LÓPEZ-MORENO ET AL., 2013). For the evaluation of meteorological

drought indices for low flow reconstruction in the non-alpine parts of Austria, HASLINGER ET AL. (2013) obtained strongest correlations between discharge and the SPI at a time scale of 4 months.

The transfer time of water from precipitation to streamflow is furthermore a function of large scale characteristics, as the comparison among all incorporated countries implies. Strength of correlation and time lag between meteorological and hydrological signals most likely reflect Europe's environmental diversity. This is furthermore illustrated by spatial patterns of the maximum linkage between the investigated indicators. Two particular features can be specified: Strongest correlations obtained for each catchment demonstrate a high level of interrelation between climatological conditions and runoff behavior across Europe, especially as aforementioned for shorter periods of the SPEI. In contrast, there are two distinct regions exhibiting a rather weak relationship between meteorological water balances and streamflow reactions. These are located at higher elevations of the Alps and the Scandinavian Mountains. This can be seen as a possible indication for the major role of ice and snow on runoff propagation in mountainous river basins.

Clusters of the continuous correlations show three contrasting patterns in terms of streamflow response times but lack a clear spatial distribution across Europe with the exception of cluster C_C5. Nevertheless, a distinction can be made between fast reacting catchments (C_C4 and C_C5), river basins with rather intermediate storage times of precipitation and catchments (C_C2 and C_C3), which exhibit rather slow response times to preceding climatic conditions (C_C1). Results show that the most contrary clusters (C_C1 and C_C5) differ strongly in terms of their physiographic characteristics, especially their size, steepness and annual amounts of precipitation. This outcome agrees with previous studies, highlighting the effects of catchment attributes on major water residence times (VICENTE-SERRANO & LÓPEZ-MORENO, 2005; VAN LANEN ET AL., 2012; LÓPEZ-MORENO ET AL., 2013). Mountainous rivers with more limited catchment areas are predominately characterized by immediate streamflow reaction to rainfall events due to their rather short and steep flow paths (SOULSBY ET AL., 2006). This can be seen as an explanation for the large number of catchments associated with cluster C_C1**,** which are located in the Northern Alps and the northern foothills of the Alps. Nevertheless, a geographical concentration of this cluster is also located in western and northern parts of the UK as well as in Western Norway. MCGUIRE & MCDONNELL (2006) identified the ma-

jor influence of groundwater storage on transfer times of water on the catchment-scale. This can be seen as a reason for the predominately azonal distribution of clusters with different correlation patterns. In consequence, the azonal character of the clusters spatial allocation demonstrates the dominant role of geology amongst other factors like climatology and aboveground basin characteristics.

The cluster analysis of the normalized discharge series provides spatially and seasonally coherent streamflow regimes. These mostly correspond well with previously obtained regime types of rivers in western and northern Europe (KRASOVSKAIA ET AL., 1994). Annual streamflow distributions mostly depend on the catchments climatic and physiographic conditions (STAHL, 2001) and can therefore be used for a more detailed assessment of the correspondence between streamflow and temporally integrated precipitation conditions. Results elucidate the effects of snow on water transfers through the terrestrial part of the hydrological cycle. In terms of continuous correlation patterns, a general distinction can be made between regimes which are more or less affected by the influence of snow and regimes which are predominately characterized by a synchronous course of climatic and hydrological conditions. The overall response of snow dominated runoff regimes to meteorological variability is comparably low and furthermore subject to large variations. These clusters exhibit relatively strong correlations at intermediate time scales of the SPEI when compared to oceanic runoff regimes, but streamflow reactions to short-term precipitation conditions (SPEI time scale of 1 month) are remarkably low. In contrast, oceanic regimes reflect the time lag between meteorological signals and runoff response without the influence and superimposition of snow and ice. Major response times are shorter and climatic and hydrological conditions exhibit a generally higher level of interrelation. These features can be interpreted as an indication for the influence of snow storage effects during winter and, subsequently, the major role of melt water runoff during the snowmelt season in spring and summer (ADAM ET AL., 2009).

5.2 Seasonal relations between the SPEI and the SSI

The correlation analysis between monthly series of the SSI and the SPEI at varying time scales gives a more specific picture of the seasonal runoff behavior with differing climatic conditions. The results show that the interrelation between monthly series of the investigated variables is more capable to specify seasonal aspects of streamflow response to climatic conditions. The correlation analysis between monthly series of the SSI and the SPEI provides a higher temporal solution of both the strength of the link as well as the temporal aspects of runoff response to climatic conditions as a function of time. Hence, the obtained clusters of seasonal linkage exhibit spatially coherent regions of common hydrological reactions to meteorological conditions at varying time scales. Additionally, results of the cluster analysis give a more detailed picture about the influence of climatological, physiographical and hydrogeological properties on natural streamflow variability. Previous studies demonstrated the major influence of groundwater, snow accumulation and melting processes as well as anthropogenic influences on streamflow responses to previous climatic conditions (LÓPEZ-MORENO ET AL., 2013). As only near natural and undisturbed catchments are incorporated, the latter effect is generally negligible in this study. Nevertheless, the major role of snow storage and hydrogeology can be confirmed.

The correlation patterns of the monthly series display the effects of snow accumulation and melting processes on streamflow variations. Runoff responses during the snowmelt season are exceptionally low when more recent conditions of the climatic water balance are considered (SPEI time scales of 1-3 months). In contrast, affected clusters tend to higher correlations with increasing time scales of the SPEI during summer, highlighting the storage properties of snow. Runoff in summer is predominately a response to precipitation conditions during winter when precipitation is stored as snow. During the season of snow accumulation there is also no linear connection between streamflow and short-term patterns of rainfall. In both cases there is no immediate reaction of river discharge on current meteorological conditions, which is indicated by the lowest correlations between the standardized variables of precipitation and current hydrological conditions during periods of snow accumulation and melting processes. In comparison, resulting patterns of seasonal correlations between the SPEI and SSI can be used to assess magnitude and temporal aspects of snow accumulation and melting processes with special regard to its hydrological impacts. In the temporal context, the

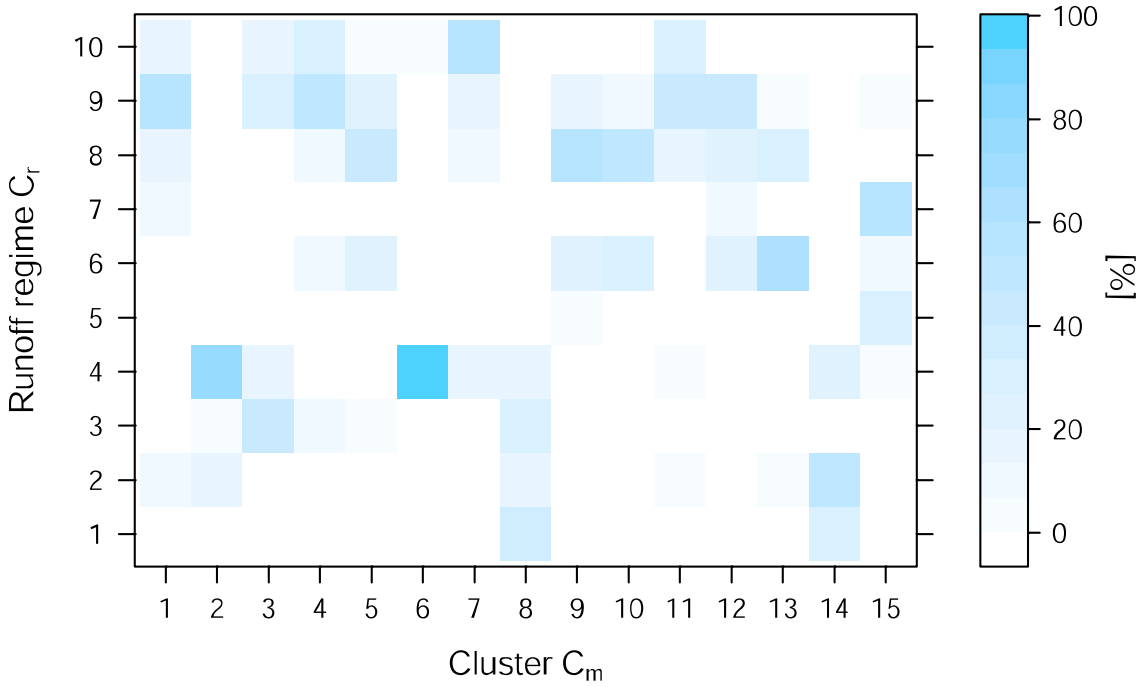

Figure 5.1: Plot of the contingency table for clusters C_m and runoff regimes C_r.

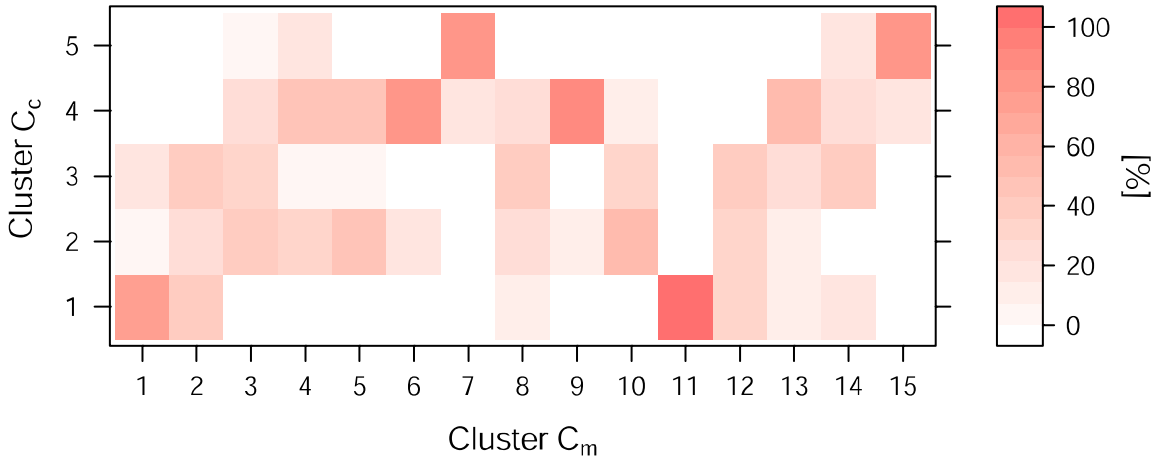

Figure 5.2: Plot of the contingency table for clusters C_m and clusters C_C.

cluster in the High Alps (C_m2) exhibits the strongest dependency on snow, as its correlations are relatively low when short time scales of the SPEI are considered with the exception of autumn. This can be explained by the high altitude of its associated catchments. The overall influence of snow is of lesser importance in the cases of clusters, which cover the Eastern Pre-Alps and the Tatra Mountains (C_m3) as well as the Northern Alps (C_m6). Patterns of seasonal correlations show both shorter periods as well as minor impacts of snow accumulation and melting processes. Even though

catchments of cluster C_m6 are on higher elevations than those of cluster C_m3, correlations between the SSI and the SPEI at short time scales begin to drop earlier in year in case of the latter classification. This demonstrates the effects of continentality on the onset of snow accumulation in winter. A minor effect of snow as a controlling factor of streamflow is also observed in case of the cluster covering the northern foothills of the Alps (C_m7). The snowmelt season in April results in relatively small correlations at short-term SPEI time scales but higher *r*-values when intermediate periods of the SPEI are taken into account. As this cluster is predominately associated to the most balanced runoff regime (C_m10), the negligible influence of snow can be explained by its stable streamflow characteristics throughout the hydrological year (STAHL, 2001). Cluster C_m14 is characterized by minimal correlation coefficients between the SSI and short-term values of the SPEI in May, which marks the latest effect of snow on streamflow among all clusters in the hydrological year. This pattern elucidates the additional influence of latitude on this phenomenon, as represented catchments of this cluster are exclusively located on higher altitudes of the Scandinavian mountains. Although its represented catchments are distributed across the Alps, the High Tatra and Scandinavia, cluster C_m8 features a common and pronounced degree of disconnection between the SSI and the SPEI at all time scales during the onset of the spring flood season. Even at the height of the snowmelt period larger time scales of the SPEI exhibit increasing relations with the SSI. The effects of snow hydrology are also observed for catchments in the lower mountain ranges of Germany and Denmark (C_m5 and C_m12) as well as in the North German Lowlands (C_m1) but play a minor role on seasonal runoff response to precipitation conditions.

Beside the effects of snow, several clusters are rather characterized by a minor seasonal influence on patterns of correlation between the monthly series of the SSI and the SPEI. In case of these clusters, the interrelation of both investigated variables seems to be more likely a function of the chosen time scales of the meteorological drought indicator. A possible explanation for the lack of seasonality in terms of the observed linkage between the indicators could be the major influence of groundwater on runoff generation throughout the hydrological year. A general distinction can be made between clusters which exhibit a direct response of streamflow to meteorological conditions and clusters which are predominately characterized by delayed streamflow reactions. This phenomenon is most pronounced in case of the cluster, which covers the Celtic region of Northwestern Europe (C_m15). As can be seen from Figure 5.1, associated catchments

are partly characterized by an Atlantic climate and related to the oceanic runoff regime (C_r7). This can be seen as an explanation for increasing coefficients of correlation at longer time scales of the SPEI during the low flow season in summer. During this period, discharge is mostly dependent on groundwater storages, formed during rainy periods in winter (HANNAFORD & MARSH, 2006). As the fjords of Western Norway (C_r5) also exhibit little influence of snow, correlations are rather weak during the snowmelt season in May when short SPEI time scales are considered. Nevertheless, seasonal influences play a minor role on the linkage between the investigated variables when compared to the effects of increasing time scales of the SPEI. As can be seen from Figure 5.2, most catchments of this classification are represented by the fast responding cluster of the continuous linkages (C_c5). This indicates that there is almost no delay of runoff throughout the year. FLEIG ET AL. (2010) described the missing basin influence on runoff generation in most regions of the UK in terms of drought propagation. They identified regions with short response times to climatic drought spells, which compare well with the geographic distribution of cluster C_m15 in case of the UK. This regionalization approves that the decline of correlations with increasing time scales of the SPEI can be seen as an indicator for missing hydrogeological storage effects. In case of the Western Norwegian catchments (C_m15), it can be assumed that there are similar hydrogeological conditions, which enhance the effects of immediate streamflow reactions to short term meteorological conditions (HANNAFORD & MARSH, 2006). Cross tabulation of seasonal and continuous relationships between the SSI and the SPEI at varying time scales also reveals the strong association of the Northern Alpine cluster (C_m7) to the fast responding cluster (C_C5) of the continuous correlation analysis. Even though there is little influence of snow during the snowmelt season, streamflow of the represented catchments tends to more current responses to climate signals. This can be attributed to the low permeability of the flysch zone in the northern parts of the mountain range (BAUER ET AL., 2003). Clusters covering the Northern Limestone Alps (C_m6) as well as the regions of the Massif Central and the Black Forest (C_m9) are also characterized by a more rapid response of streamflow, as they are mostly represented by cluster C_c4. Associated catchments exhibit both short and intermediate response times to climate conditions throughout the year. This can be attributed to their common geological settings. Both regions are underlain by rather impermeable rock formations of Variscan fault structures and near-surface layers of glacial debris (ARBOS, 1922; BORCHERT, 1991). This stratification leads to a combination of interflow and direct runoff. In case

of cluster C_m6 the tendency towards fast streamflow responses to precipitation conditions is furthermore influenced by the superimposed effects of snow accumulation and melting processes.

In contrast to those clusters, which are characterized by rather short-term runoff reactions to climatic variations, several clusters exhibit a pronounced degree of delayed hydrological response. This effect is found to be strongest amongst those catchments, which belong to cluster C_m11, but can also be observed in cases of cluster C_m1 and cluster C_m12. The lack of seasonality and increasing interrelation between standardized values of discharge and the climatic water balance can be seen as an indicator for the major role of hydrogeological "buffering" effects. An additional indication for this interpretation could be the large spatial heterogeneity of associated catchments**,** which are in both cases situated in differing climatic regimes. This outcome elucidates that short-term climatological conditions and their temporal variability play a minor role on runoff generation, which agrees with results of previous studies: ZAIDMANN & REES (2000) highlighted the importance of groundwater on patterns of streamflow during low flow periods in the chalk plains of southern England and northern France. Northern parts of Germany and Denmark are also characterized by highly productive aquifers delaying the response of streamflow to climate drivers (STAHL, 2001; FLEIG ET AL., 2010). The influence of groundwater storage on streamflow reaction becomes less apparent in cases of cluster C_m1 and cluster C_m12, which are both not exclusively associated with the slow responding cluster of continuous linkage (C_C1) and, additionally, shows effects of snow accumulation and melting processes during winter and early spring due to its geographical distribution. During summer and autumn surface runoff is predominately a function of long-term moisture conditions as constantly high correlations for intermediate and long SPEI time scales indicate. The hydrological response during these periods is therefore governed by both current and long-term precipitation conditions. This can be explained by the increasing influence of groundwater on runoff generation when the effects of snowmelt are no longer effective in cases of mountainous (C_m2, C_m3, C_m5, C_m6, C_m8, C_m12) and Scandinavian clusters (C_m8, C_m12, C_m14) or the height and offset of the dry season leads to an increased proportion of base-flow to the overall river discharge (C_m10 and C_m15). The latter effect can also be observed for those clusters which are characterized by the influence of snow. STAHL (2011) elucidated spatial variations of months with the lowest river flow across Europe. As most catchments in Europe exhibit their period of low discharge during summer and au-

tumn, the high levels of correlation at intermediate and long-term time scales of the SPEI demonstrate the major role of base flow during the low flow season.

6 Conclusion

This study highlights the applicability of meteorological drought indicators for the explanation of streamflow patterns across different environmental and seasonal conditions. To ensure comparability between the climatic and hydrological variations over space and time, the computation of a standardized and normalized streamflow index was applied. The linkage between climatic variations at varying time scales and runoff behavior of near-natural streams provides a clear indication about the temporal aspects of water transfer and storage on the catchment scale. It could be elucidated that streamflow response to changing weather conditions can be seen as a function of (i) hydrological drought states and (ii) temporal aggregations of the meteorological water balance as well as (iii) large and small-scale properties of the respective catchment. The results confirm a strong regional character of monthly streamflow responses to short and long-term climatic conditions. It could be illustrated that spatiotemporal differences and similarities of the interrelation between climatic and hydrological indicators are mostly influenced by snow and groundwater. Nevertheless, this study has several limitations. Unfortunately, no high resolution data about the hydrogeological properties of the incorporated catchments was available for this thesis. As the results indicate the major role of groundwater interaction on streamflow response, the complex monthly correlation patterns can only be explained in part. Moreover, further research should be conducted in the multidimensional character of the investigated linkage. In the course of this thesis, the conducted analyses incorporated not only the SPEI, but also the SPI. As the derived results only showed minor differences and to not exceed the framework of this study, only the SPEI was incorporated in the final assessment. Nevertheless, the role of evaporation on the investigated interrelations remains to be explained more in detail. The influence of hydrological conditions was only partly incorporated in this study. It remains to be determined how seasonal and regional patterns of runoff response are influenced by differing streamflow thresholds. The same applies to different states of the meteorological water balance in the form the SPEI. In conclusion, the high explanatory power of meteorological drought indicators in relation to seasonal streamflow patterns provides new opportunities for water management. Their standardized, normalized and multi-temporal character can be applied to estimate the amount of usable river water resources.

References

Abramowitz, M. & Stegun, I.A. (1965): Handbook of Mathematical Functions. Dover Publications, New York.

Arbos, P. (1922) : Le Glaciaire dans le Massif Central. Revue de géographie alpine: 481-487.

Arnell, N.W., Krasovskaia, I. & Gottschalk, L. (1993): River flow regimes in Europe. In: Flow Regimes fromInternational Network Data (FRIEND). Volume I - Hydrological Studies. Institue of Hydrology. Wallingford. UK.

Bauer, J., Bohl, E., Schneider, S., Lehmann, R., Foeckler, F., Deichner O., Krois, A., Kifinger, B., Hüfmann, C., Hubmann, M., Künz, E., Moritz, C., Ritzenfeld, T., Depisch, C. & Robrecht, D. (2003): Integrierte ökologische Bewertung von bayerischen Fließgewässern südlich der Donau. Materialien des LfW-Bayern, Nr. 109, mit cd-Anhang. München.

Borchert, C. (1991): Baden-Württemberg. Eine geographische Landeskunde. Wissenschaftliche Länderkunden 8. Wissenschaftliche Buchgesellschaft, Darmstadt.

Cancelliere, A., Loukas, A., Pangalou, D., Rossi, G., Tigkas, D., Tsakiris, G. & Vangelis, H. (2007): Drought characterization (Part 1. Components of drought planning. 1.3. Methodological component). In: Iglesias, A., López-Francos, A., Moneo, M. (Eds.), Drought management guidelines technical annex. Options Méditerranéennes : Série B. Etudes et Recherches. Zaragoza : CIHEAM / EC MEDA Water, pp. 85-102.

Chow, V.T., Maidment, D.R., & Myas, L.W. (1988): Applied Hydrology. MacGraw-Hill. New York.

García-Ruiz, J.M., Regüés, D., Alvera, B., Lana-Renault, N., Serrano-Muela, P., Nadal-Romero, E., Navas, A., Latron, J., Martí-Bono, C. & Arnáez, J. (2008): Flood generation and sediment transport in experimental catchments affected by land use changes in the central pyrenees. J. Hydrol. 356 (1–2), 245–260.

Gibbs, W.J., & Maher, J.V. (1967): Rainfall Deciles as Drought Indicators. Australian Bureau of Meteorol-ogy, Bull. 48.

Guttman, N.B. (1998): Comparing the Palmer Drought Index and the Standardized Precipitation Index. Journal of the American Water Resources Association, 34(1): 113-121.

Haslinger K., Koffler D., Blöschl G., Parajka J., Schöner W. & Laaha G. (2013): Exploring the link between meteorological drought indices and streamflow with emphasis on low flows. Submitted to Water Resources Research.

Hosking, J.R.M., Wallis, J.R. & Wood, E.F., (1985): Estimation of the generalized extreme-value distribution by the method of probability-weighted moments. Technometrics, 27: 251-261.

Hosking, J.R.M. (1986): The theory of probability weighted moments. Research Report RC12210. IBM Research Division, Yorktown Heights, NY.

Hosking, J.R.M. (1990): L-Moments: Analysis and Estimation of Distributions Using Linear Combinations of Order Statistics. Journal of the Royal Statistical Society. Series B (Methodological), 52(1): 105-124.

Krasovskaia, I., Arnell, N.W. & Gottschalk, L. (1994): Flow regimes in northern and western Europe: develop-ment and application of the procedures for classifying flow regimes. In: FRIEND: Flow Regimes fromInternational Experimental and Network Data (ed. by P. Seuna, A. Gustard, N.W. Arnell & G.A. Cole), 179-184. IAHS Publ. no. 221.

Latron, J. & Gallart, F. (2008): Runoff generation processes in a small mediterranean research catchment (Vallcebre, Eastern Pyrenees). J. Hydrol. 358, 206–220.

López-Moreno, J.I., Vicente-Serrano, S.M., Beguería, S., García-Ruiz, J.M., Portela, M.M. & Almeida, A.B. (2009) : Dam effects on droughts magnitude and duration in a transboundary basin: The Lower River Tagus, Spain and Portugal. Water Resources Research, 45(2): W02405.

López-Moreno, J.I. Vicente-Serrano, S.M., López-Moreno, J.I., Beguería, S., García-Ruiz, J.M. & Cuadrat, J.M. (2013): Hydrological response to climate variability at different time scales: A study in the Ebro basin. Journal of Hydrology, 477(0): 175-188.

Lorenzo-Lacruz, J., Vicente-Serrano, S.M., López-Moreno, J.I., Beguería, S. & Garcia-Ruiz, J.M. (2010): The impact of droughts and water management on various hydrological systems in the headwaters of the Tagus River (central Spain). Journal of Hydrology, 386(1–4): 13-26.

Lorenzo-Lacruz, J., Morán-Tejeda, E., Vicente-Serrano, S.M. & López-Moreno, J.I. (2012): Streamflow droughts in the Iberian Peninsula between 1945 and 2005: spatial and temporal patterns. Hydrol. Earth Syst. Sci. Discuss., 9(7): 8063-8103.

McDonnell, J.J., McGuire, K., Aggarwall, P., Beven, K.J., Biondi, D., Destouni, G., Dunn, S., James, A., Kirchner, J., Kraft, P., Lyon, S., Maloszewski, P., Newman, B., Pfister, L., Rinaldo, A., Rodhe, A., Sayama, T., Seibert, J., Solomon, K., Soulsby, C., Stewart, M., Tetzlaff, D., Tobin, D., Troch, P., Weiler, M., Western, A., Wörman, A. & Wrede, S. (2010): How old is streamwater? Open questions in catchment transit time conceptualization, modelling and analysis. Hydrol. Process. 24, 1745–1754.

Morin, E., Enzel, Y., Shamir, U. & Garti, R. (2001): The characteristic time scale for basin hydrological response using radar data. Journal of Hydrology, 252(1–4): 85-99.

Nalbantis, I. & Tsakiris, G. (2009): Assessment of Hydrological Drought Revisited. Water Resour Manage, 23(5): 881-897.

Pardé, M. (1933): Fleuves et rivières. Collins. Paris.

Post, D.A. & Jakeman, A.J. (1996): Relationships between catchment attribute and hydrological response characteristics in small Australian mountain ash catchments. Hydrological Processes, 10(6): 877-892.

Rencher, A.C. (2002): Methods of Multivariate Analysis. Wiley & Sons, Inc.

Shukla, S. & Wood, A.W. (2008): Use of a standardized runoff index for characterizing hydrologic drought. Geophysical Research Letters, 35(2): L02405.

Siegel, S., & Castelan N.J. (1988): Nonparametric Statistics for the Behavioral Sciences, McGraw-Hill, New York.

Singh, V.P. & Guo, F.X.Y. (1993): Parameter estimation for 3-parameter log-logistic distribution (LLD3) by Pome. Stochastic Hydrology and Hydraulics, 7: 163-177.

Soulsby, C., Tetzlaff, D., Rodgers, P., Dunn, S. & Waldron, S. (2006): Runoff processes, stream water residence times and controlling landscape characteristics in a mesoscale catchment: an initial evaluation. J. Hydrol. 325, 197–221.

Stahl, K. (2001): Hydrological drought—a study across Europe. Albert-Ludwigs Universität Freiburg: Geowissenschaftlichen Fakultät. Freiburg. 114 pp.

Szalai, S., Szinell, C. S., & Zoboki, J. (2000): Drought monitoring in Hungary, in: Early warning systems for drought preparedness and drought management, World Meteorological Organization, Lisboa, 182–199.

Van Lanen, H.A.J., Wanders, N., Tallaksen, L.M. & Van Loon, A.F. (2012): Hydrological drought across the world: impact of climate and physical catchment structure. Hydrol. Earth Syst. Sci. Discuss., 9(10): 12145-12192.

Van Loon, A.F. (2013): On the propagation of drought. How climate and catchment characteristics influence hydrological drought development and recovery. PhD thesis. Wageningen University, Wageningen. 196 pp.

van Rooy, M.P. (1965): A rainfall anomaly index independent of time and space. Notos, Weather Bureau of South Africa, 14: 43-48.

Vasiliades, L. & Loukas, A. (2009): Hydrological response to meteorological drought using the Palmer drought indices in Thessaly, Greece. Desalination, 237(1–3): 3-21.

Vicente-Serrano, S.M. & López-Moreno, J.I. (2005): Hydrological response to different time scales of climatological drought: an evaluation of the Standardized Precipitation Index in a mountainous Mediterranean basin. Hydrol. Earth Syst. Sci., 9(5): 523-533.

Vicente-Serrano, S.M. (2006): Differences in Spatial Patterns of Drought on Different Time Scales: An Analysis of the Iberian Peninsula. Water Resour Manage, 20(1): 37-60.

Vicente-Serrano, S.M., Beguería, S. & López-Moreno, J.I. (2009): A Multiscalar Drought Index Sensitive to Global Warming: The Standardized Precipitation Evapotranspiration Index. Journal of Climate, 23(7): 1696-1718.

Vicente-Serrano, S.M., López-Moreno, J.I., Beguería, S., Lorenzo-Lacruz, J., Azorin-Molina, C. & Morán-Tejeda, E. (2012a): Accurate Computation of a Streamflow Drought Index. Journal of Hydrologic Engineering, 17(2): 318-332.

Vicente-Serrano, S.M., Beguería, S., Lorenzo-Lacruz, J., Camarero, J.J., López-Moreno, J.I., Azorin-Molina, C., Revuelto, J., Morán-Tejeda, E. & Sánchez-Lorenzo, A. (2012b): Performance of Drought Indices for Ecological, Agricultural, and Hydrological Applications. Earth Interactions, 16(10): 1-27.

Vidal, J.P., Martin, E., Franchistéguy, L., Habets, F., Soubeyroux, J.M., Blanchard, M. & Baillon, M. (2010): Multilevel and multiscale drought reanalysis over France with the Safran-Isba-Modcou hydrometeorological suite. Hydrol. Earth Syst. Sci., 14(3): 459-478.

Vogt, J. V., Soille, P., de Jager, A. L., Rimaviciute, E., & Mehl, W. (2007): A pan-European river and catchment database. EC-JRC. 120pp.

Wilhite, D.A. & Glantz, M.H. (1985): Understanding: the Drought Phenomenon: The Role of Definitions. Water International, 10(3): 111-120.

Zaidman, M.D., Rees, H.G. & Young, A.R. (1999): Spatio-temporal development of streamflow droughts in north-west Europe. Hydrol. Earth Syst. Sci., 6(4): 733-751.

Zhai, J., Buda, S., Krysanova, V., Vetter, T., Gao, C. & Jiang, T. (2010): Spatial Variation and Trends in PDSI and SPI Indices and Their Relation to Streamflow in 10 Large Regions of China. Journal of Climate, 23(3): 649-663.

Abbreviations

C_C	Clusters of correlations between the continuous SSI and SPEI series
C_m	Clusters of correlations between the monthly SSI and SPEI series
C_r	Runoff regimes
CCM	River and Catchment Database for Europe
Drought-R&SPI	Fostering European Drought Research and Science-Policy Interfacing
EU	European Union
EWA	European Water Archive
FRIEND	Flow Regimes from International Experiment and Network Data
GRDC	Global Runoff Data Center
IHP	UNESCO's International Hydrological Programme
PDSI	Palmer Drought Severity Index
RAI	Rainfall Anomaly Index
SDI	Streamflow Drought Index
SPEI	Standardized Precipitation Evapotranspiration Index
SPI	Standardized Precipitation Index
SRI	Standardized Runoff Index
SSI	Standardized Streamflow Index
UNESCO	United Nations Educational, Scientific and Cultural Organization
WATCH	Water and Global Change

Symbols

α	Gamma shape parameter of the log-logistic distribution
α	scale parameter of the cumulative Generalized Pareto distribution and Weibull distribution function
α	significance level
β	Gamma scale parameter of the log-logistic distribution
b	shape parameter of the cumulative Weibull distribution function
Γ	Gamma function
γ	Gamma location parameter of the log-logistic distribution
C	constant for parameter estimation of the Generalized Extreme Value and Weibull distribution
C_x	constant x for standardization
C_x	cluster
c_j	centroid of characteristic values within one of the particular clusters k
$CDF(x_i)$	cumulative empirical and theoretical distribution functions
σ	shape parameter of the cumulative lognormal distribution function
D	D-statistic of the Kolmogorov-Smirnoff test
Dw	Ward-distance
$d_{p,i}$	Pearson's distance measure
d_{x}	constant x for standardization
ε	location parameter of the cumulative Generalized Pareto distribution function
e	Euler's number
erf	Gaussian error function

Φ	standard normal distribution function
$F(x)$	cumulative distribution function
F_i	frequency estimator for a specific discharge value of rank i
H_0	null hypothesis of the Kolmogorov-Smirnoff test
H_a	alternative hypothesis of the Kolmogorov-Smirnoff test
i	rank
κ	shape parameter of the cumulative Generalized Extreme Value distribution function
λ_x	L-moments of discharge series x
ln	natural logarithm
μ	log-scale parameter of the cumulative Generalized Extreme Value and the lognormal distribution function
μ	location parameter of the distribution function
m	raw moment of the empirical distribution function
max_i	maximum vertical difference between the tested functions for a specific value i
n	number of datapoints in the k-means clustering algorithm
n	number of observations
n_x	number of objects in cluster x
π	Pi
P	exceedance probability of a specific discharge value
$PC_{m(i)}$	Pardé-coefficient of month i
$\bar{Q}_a$	annual mean discharge [$m^3\ s^{-1}$]
$\bar{Q}_{m(i)}$	mean discharge of month i [$m^3\ s^{-1}$]

r	rank of the specific observation
r_i	Pearson's correlation coefficient
r-value	Pearson's correlation coefficient
τ_m	m^{th} L-moment ratio
τ_3	L-skewness
τ_4	L-kurtosis
ω_x	probability weighted moments of the discharge series x
W	target value for z-scoring
x_i	SPEI value
$\bar{x}$	average SPEI value
$\bar{x}_x$	arithmetic means of all objects of n objects in cluster x
$x_{i,j}$	datapoint consisting of 12 monthly Pardé-coefficients
y_i	SSI value
$\bar{y}$	average SSI value
z	estimator for the log-scale parameter of the log-normal distribution